Journal of Materials Research and Technology 33 (2024) 3501–3517

Contents lists available at ScienceDirect

Journal of Materials Research and Technology

journal homepage: www.elsevier.com/locate/jmrt

Electroplasticity constitutive modeling of aluminum alloys based on dislocation density evolution

Yanli Song [a,b,c,1,*], Long Chen [a,b,1], Chuanchuan Hao [a,b], Lin Hua [a,b,c,**], Hainan Xu [a,b], Jue Lu [a,b,***], Zhongmei Wang [a,b], Jianguo Lin [d], Yanxiong Liu [a,b,c], Lechun Xie [a,b,c]

[a] Hubei Key Laboratory of Advanced Technology for Automotive Components, Wuhan University of Technology, Wuhan, 430070, China
[b] Hubei Collaborative Innovation Center for Automotive Components Technology, Wuhan University of Technology, Wuhan, 430070, China
[c] Hubei Research Center for New Energy & Intelligent Connected Vehicle, Wuhan University of Technology, Wuhan, 430070, China
[d] Department of Industrial and Systems Engineering, The Hong Kong Polytechnic University, Hung Hom, Kowloon, Hong, China

ARTICLE INFO

Handling editor:SN Monteiro

Keywords:
Electroplasticity
Constitutive model
Aluminum alloy
Ratchet shape mechanical behavior
Dislocation density evolution

ABSTRACT

Electrical current can effectively improve the plasticity of metallic materials. The tensile deformation behavior of Al alloys under the pulsed electrical current assisted quasi-static unidirectional tension (EAT) has been investigated. Materials under the EAT exhibits periodic electro-softening and strain-hardening behaviors, i.e., a ratchet shape mechanical response. However, establishing a constitutive model to accurately predict the ratchet shape mechanical behavior, especially during the EAT interval, and accurately predicting the strain-hardening behavior of materials are critical issues that need to be solved urgently. In this study, based on the Taylor polycrystalline model, thermal activation theory and dislocation density evolution theory, a two-parameter dislocation density electroplasticity constitutive model with forward and reverse dislocation density evolution was developed to describe the periodic coupling effect of the electro-thermal-mechanical fields during EAT. The tensile deformation behaviors of AA 6061-T6 and AA 7075-T6 under the effect of a pulsed electrical current were quantitatively predicted using the proposed constitutive model. The results show that the correlation coefficient between the predicted and experimental results of the constitutive model can reach 0.84–0.99, implying that the proposed constitutive model can accurately predict the complex electroplasticity behavior of Al alloys during EAT.

Nomenclature and abbreviation definition

M	Taylor factor
σ	Flow stress
ε_p	Plastic strain
τ	Critical shear stress of the activated slip systems
γ	Shear strain of the activated slip system
$\dot{\gamma}_p$	Shear plastic strain rate
$\dot{\gamma}_0$	Pre-exponential factor
k	Boltzmann constant
T	Thermodynamic temperature
ΔG	Gibbs free energy
ΔF	Total activation energy is required for the dislocation to cross the barrier
$\widehat{\tau}$	A material property called the mechanical threshold
ρ	Dislocation density
τ_0	Lattice resistance
μ	Shear modulus of elasticity
α	Material constant that measures the interaction between dislocations
b	Length of Burgers vector
K_1	Dislocation storage coefficient
K_2	Dislocation dynamic recovery coefficient
K_{20}	Dislocation dynamic recovery factor
$\dot{\varepsilon}_0$	Strain rate factor
n	Strain rate index

(continued on next column)

(continued)

(continued on next page)

* Corresponding author. Hubei Key Laboratory of Advanced Technology for Automotive Components, Wuhan University of Technology, Wuhan, 430070, China.
** Corresponding author. Hubei Key Laboratory of Advanced Technology for Automotive Components, Wuhan University of Technology, Wuhan, 430070, China.
*** Corresponding author. Hubei Key Laboratory of Advanced Technology for Automotive Components, Wuhan University of Technology, Wuhan, 430070, China.
E-mail addresses: ylsong@whut.edu.cn (Y. Song), hualin@whut.edu.cn (L. Hua), lujue@whut.edu.cn (J. Lu).
[1] Equal contributions.

https://doi.org/10.1016/j.jmrt.2024.09.238
Received 30 July 2024; Received in revised form 24 September 2024; Accepted 28 September 2024
Available online 2 October 2024

(*continued*)

ρ_0	Initial dislocation density
λ	Diffraction wavelength of Cu $K\alpha$
D	Average microcrystal size
ε_{micro}	Average microstrain
F_{ew}	Electron wind force
ρ_f	Forward dislocation density
ρ_r	Reverse dislocation density
i-th	i-th pulse period
ε^i	Strain at the end of the electrical current in the i-th pulse period
ρ_f^i	Total dislocation density when the specimen is strained to ε^i
ρ_{total}	$\rho_{total} = \rho_f - \rho_r$
$\rho_f(\varepsilon_p{}^i)$	Forward dislocation density when the specimen is strained to ε^i
$\rho_r(\varepsilon_p{}^i)$	Reverse dislocation density when the specimen is strained to ε^i
J	Electrical current density
ω	Pulse period
$\dot{\varepsilon}_p$	Strain rate
t_d	Pulse duration
t_i	Pulse interval
p、q	Obstacle distribution parameters
S	A scalar quantity, representingthe percentage of the total dislocation density converted to reverse dislocation density when the electrical current ends
H	Ascalar, representing the evolution rate of the reverse dislocation density
R	Correlation coefficient between the test results and the predicted results
α_0、β_1、β_4、β_5	Parameters related to temperature and strain rate
β_2、β_3、β_6、β_7	Parameters connected to electrical current density
EAT	electrical current assisted quasi-static unidirectional tension
DC	direct current
2D	two-dimensional
EST	electroshock treatment
NC	no electrical current
RT	room temperature
FCC	face-centered cubic
GP	Guinier-Preston
F_{ew}	electron wind force
FWHM	full width at half maximum
XRD	X-Ray Diffraction
EST	electroshock treatment
DAQ	Data acquisition
AARE	average relative errors
RMSE	root mean square error

1. Introduction

Al alloys have become one of the primary lightweight materials for aerospace, high-speed rail, automobile, and other transportation equipment owing to their advantages of low density, high specific strength, good corrosion resistance, and excellent collision energy absorption [1,2]. In conventional forming approaches, the main challenge in forming complex-shaped parts of Al alloys is their poor deformability, mainly caused by their relatively low plasticity [3,4]. Therefore, novel forming methods for complex Al alloy components have attracted extensive research attention [5].

Pulsed electrical current assisted forming is a new type of material-processing technology that has emerged in recent years [6]. Applying a certain electrical current field in the traditional plastic forming process can help reduce the deformation resistance of the material and improve formability [7,8]. These advantages promote the industrial applications of the technology; some electrical current assisted forming processes, such as stamping [9], forging [10], and rolling [11], are currently being studied.

Literature reviews have revealed that research on the mechanical behavior and mechanism of metal materials under the action of an electrical field has been ongoing since the mid-20th century. In the 1970s, the influence of the electroplasticity effect on the yield stress, plastic deformation, and creep of pure metals such as zinc and tin was reported by Troitskii [12] and Troitskii et al. [13,14]. Under the action of a direct current (DC), the yield stress of metal materials decreases. Then, the movement of dislocations are significantly enhanced, and the creep speed increases [12,15]. For metals such as 2024-T4 Al alloy, C11000 Cu alloy, and 130 B Ti alloy, DC can reduce flow stress and elongation during tensile deformation [16,17]. However, existing research has shown that the improvement in the plasticity of some materials may be limited by the use of DC assisted deformation. Moreover, the Joule heating phenomenon is severe when a continuous electrical current is applied, and the temperature increases rapidly. For temperature-sensitive materials such as Al alloys, it is difficult to accurately control the temperature, which can easily cause adverse consequences such as overburning.

Unlike the plasticity improvement brought about by the thermal softening generated by DC, the application of pulsed electrical current can effectively improve the plasticity of materials even at relatively low temperatures. Roth et al. [18] and Salandro et al. [19] studied the effect of a pulsed electrical current on the elongation of 5052-H32, 5083-H32, and 5754-H32 Al alloys sheets, finding that the elongation of these three Al alloys increased by 54.3%, 90.6%, and 300%, respectively. In addition, Zhou et al. [20] showed that a pulsed electrical current could accelerate the dissolution of particles in an Al–Cu–Li alloys, increase the vacancy concentration, and promote evolution from the initial helical dislocations to straight lines, i.e., dislocation reconstruction, with the final creep strain increased by approximately 12 times. Interestingly, Lee et al. [21] and Kim et al. [22] found that, during pulsed electrical current assisted uniaxial tension, the stress–strain curves of Al alloys exhibited a periodic stress drop-stress recovery phenomenon with a change in the pulsed electrical current, resulting in a typical ratchet shape. The above studies highlight complex interactions between the pulsed electrical current and the microstructure of the material [23], such as accelerating atomic diffusion [24], promoting particle dissolution [25], changing the dislocation configuration [26] and altering the dislocation motion mode [27].

Although the phenomenon of electroplasticity in materials has been widely accepted, the physical mechanisms underlying electroplasticity have not been unified. The physical mechanism of electroplasticity mainly includes Joule heating [28,29], electron wind [30,31], magnetic depinning [32,33], and the recently proposed atomic vibrations [34].

The increase in deformation resistance caused by the hindrance of dislocation movement is a key problem in the field of plastic deformation of materials. To quantitatively describe the complex stress–strain dynamic response relationship between dislocations and the microstructure, establishing a correct plastic constitutive equation is crucial. Krasnikov et al. [35] developed a three-stage technique combining atomic calculations, a parametric dislocation-precipitation interaction model, and two-dimensional (2D) dislocation dynamics to determine the flow stresses of Al alloys. The results demonstrated that the predicted flow stress values were consistent with the experimental results. Santos-Güemes et al. [36] analyzed the interaction mechanism between precipitates and dislocations in Al–Cu alloys with discrete dislocation dynamics and revealed that the predicted critical resolved shear stress was consistent with the experimental results and that the stress-free phase transformation strain contributed the most to precipitation hardening. The above two models establish a good connection between crystal dislocations and macroscopic mechanical behavior. However, because of the softened behavior of metal materials under the action of a pulsed electrical current, these models cannot be used to predict the electroplasticity behavior of materials during electrical current assisted quasi-static unidirectional tension (EAT). For a long time, the mechanical response behavior during pulsed electrical current-assisted deformation was believed to be mainly caused by the Joule heat effect. Roh et al. [37] conducted simulations of the mechanical behavior of 5052-H32 Al alloys assisted by a pulsed electrical current using a model constructed by the Joule heat effect and an empirical expression equation. The results illustrated that the model could predict the upper boundary of the ratchet shape stress–strain curve. Wang et al. [38] developed a thermomechanical constitutive model based on the Joule heat effect and flow stress model; the developed model could predict the

thermal and mechanical behaviors of AZ31 Mg alloys under pulsed electrical current-assisted deformation to a certain extent. However, constitutive models based on the Joule heat effect are not sufficient to simulate the instantaneous stress drop behavior of metallic materials during the action of a pulsed electrical current. To overcome these challenges, Kim et al. [39] predicted the electroplasticity behavior of Al–Mg–Si alloys based on the Kocks–Mecking–Estrin dislocation density model and the precipitation hardening model. The results indicated that this constitutive model could depict the peak flow stresses of Al–Mg–Si alloys at the instant of pulsed electrical current action. Liu et al. [40] proposed a multiscale constitutive model based on the dislocation density model and various strengthening mechanisms to describe the deformation behavior of electrical current assisted Ni-based superalloys. The development model could effectively predict the electrical current-assisted tension force of thin-walled Ni-based superalloy capillaries. Zhao et al. [41] and Gao et al. [42] conducted similar attempts to couple dislocation density models, thermal effects, and various strengthening mechanisms; these models could predict the mechanical behavior of the material under the electro-thermal-mechanical effect. However, as the strain-hardening behavior during the pulsed electrical current interval was not considered, it was impossible to describe the ratchet shape mechanical response behavior under pulsed electrical current-assisted uniaxial tension. The two-parameter dislocation density model can capture the complex mechanical behavior of materials under periodic loading [43], which is positive to describe the mechanical response behavior of stress drop and strain-hardening. Based on these investigations, Hariharan et al. [44] further proposed a two-parameter (i.e., forward and reverse dislocations) dislocation density constitutive model to predict the mechanical response behavior of 5052 A l alloys under pulsed electrical current and proved that the model could effectively determine the instantaneous stress drop behavior of AA5052 under pulsed electrical current and the stress recovery behavior at intervals of pulsed electrical current. Tiwari et al. [45] predicted the electroplasticity behavior of AA 6061-T6 by establishing a fully coupled constitutive model based on the thermal and two-parameter dislocation density; this model was demonstrated to be effective in predicting the instantaneous stress drop, stress recovery during electrical current removal, and long-range thermal softening behavior. The results of the above studies revealed that a two-parameter dislocation density constitutive model based on the physical mechanism of dislocation density can effectively predict the ratchet shape mechanical response behavior of materials. However, most of the electrical current electroplasticity constitutive models based on dislocation density evolution are built on the macroscopic continuum assumption, and their predictive accuracy can be further improved. Moreover, current research mostly focuses on individual materials with similar electroplasticity behavior, and there is no universality verification of the constitutive model in multiple materials, which limits the application of the electroplasticity constitutive model based on dislocation density. In the present work, a novel two-parameter dislocation density model is proposed to capture the complex ratchet shape mechanical responses of Al alloys under EAT conditions based on the microscopic Taylor polycrystalline model, thermal activation theory, and dislocation density evolution theory, with the deformation processes of AA 6061-T6 and AA 7075-T6 under EAT with different electrical current parameters and strain rates used to verify the accuracy of the proposed model.

2. Materials and experiments

2.1. Experimental materials

Commercial AA 6061 in the T6 state (2.0 mm thickness) and commercial AA 7075 in the T6 state (1.6 mm thickness) were used as the test materials. The nominal chemical compositions of the Al alloys are listed in Table 1. A special specimen with screw holes at both ends was designed to facilitate the connection between the specimens and electrodes. Fig. 1 depicts the specimen dimensions and actual product. The tensile specimens were prepared by laser cutting along the rolling direction of the sheets.

2.2. EAT processing

A pulsed electrical current assisted tensile platform was built using an electronic universal tensile testing machine (CMT-5205), DC power supply (ZX7-630A), and infrared thermometer (Fotric 226), as shown in Fig. 2. The pulsed electrical current waveform during EAT is shown in Fig. 3. A unidirectional square wave with constant electrical current density and period was used in EAT. The pulsed electrical current used in our research has the characteristics of high energy density, extremely low frequency, a unidirectional positive pulse, and very limited treatment time. This new process was referred to as the electroshock treatment (EST) in our previous studies [46,47]. In addition, the duration, interval, and pulse period were adjusted during EAT. Moreover, an insulating gasket was added inside the tension chuck to ensure sufficient insulation between the specimen and testing machine. In this work, 12 sets of EAT tests were conducted on AA 6061-T6 and AA 7075-T6 by combining different electrical current densities (J), pulsed electrical current durations (t_d), pulsed electrical current interval (t_i), pulse periods (ω) and strain rates ($\dot{\varepsilon}_{\mathbf{p}}$). The detailed parameter sets are listed in Table 2. To verify the repeatability of the results, at least three specimens were tested per set. The test results of No. 1 and No. 7 in Table 2 were used to analyze the mechanical behavior of the EAT and solve the parameters of the subsequently proposed constitutive model. The others were used to verify the universality of the constitutive model. In each test set, the first pulsed electrical current was applied after the plastic deformation of the material. A thermal infrared imager was used to monitor the surface temperature of the specimens dynamically during the entire testing process. Fig. 4 shows the thermal infrared images and temperature-time curves of the specimens during EAT for some typical cases. For example, the peak temperature of AA 6061-T6 specimens with a parameter of 50 A/mm^2-1s–30s was 67.2 °C; the average temperature was 34.5 °C (Fig. 4(a)). For AA 7075-T6, the peak surface temperatures are 70.4 °C, the average temperature was 32.9 °C (Fig. 4(b)). Thus, these results indicate a limited increase in the average temperature of the specimens during the EAT process. The reason for strictly controlling temperature rise in these cases is to develop a plastic deformation process for high-strength Al alloys at near room temperature (RT), avoiding heat damage.

3. Plastic deformation behavior of Al alloys during EAT

Figs. 5 and 6 show the true stress–true strain curves of AA 6061-T6 and AA 7075-T6 under different strain rates and pulsed electrical current parameters, respectively. The results demonstrate that the true stress–true strain curves of AA 6061-T6 and AA 7075-T6 under the action of EAT exhibit a ratchet shape. It is clearly different from the results

Table 1
Nominal chemical compositions of AA 6061-T6 and AA 7075-T6 sheets (wt.%).

Composition	Si	Fe	Cu	Mn	Mg	Cr	Zn	Ti	Al
6061-T6	0.62	0.20	0.22	0.08	0.92	0.28	0.15	0.100	Bal.
7075-T6	0.40	0.35	1.52	0.092	2.66	0.22	5.28	0.029	Bal.

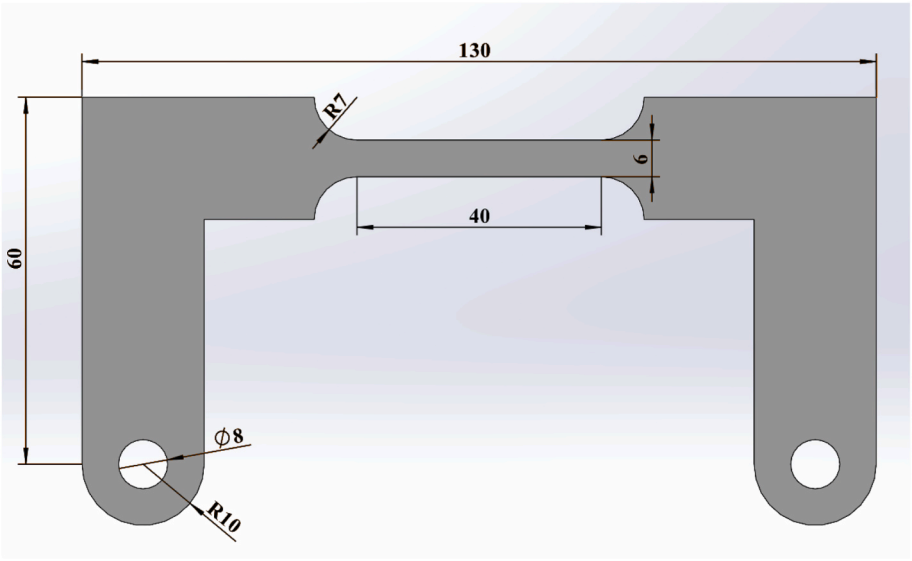

Fig. 1. Dimensions of the EAT specimens (unit: mm).

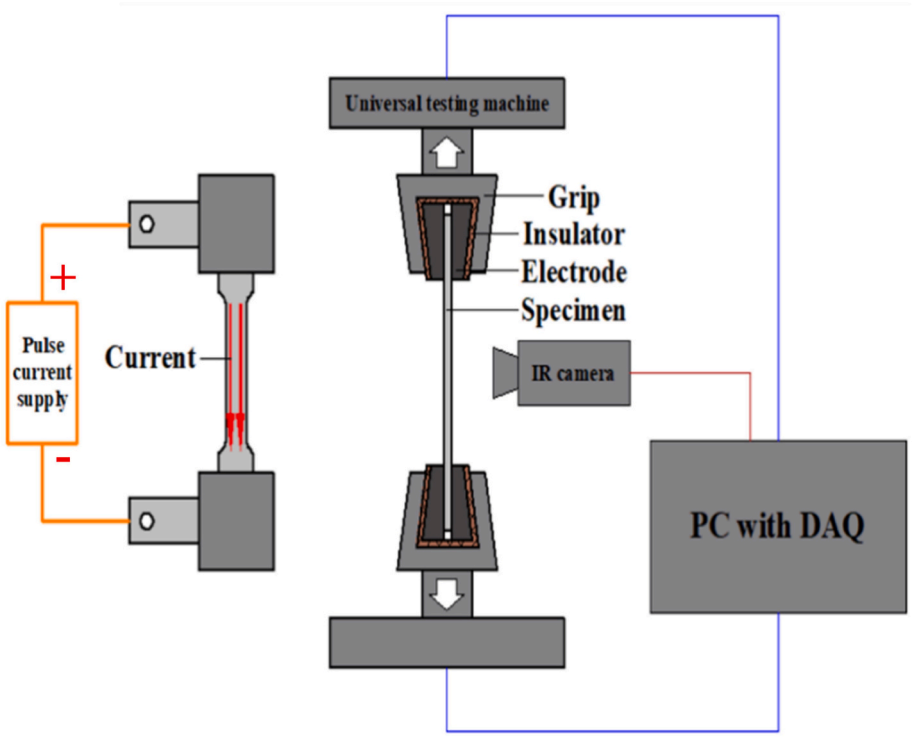

Fig. 2. The schematic diagram of EAT Platform. Data acquisition: DAQ.

of the no electrical current (NC) tensile tests. During the pulsed electrical current duration stage, a significant electro-softening phenomenon on the flow stress of the Al alloys was observed owing to the coupling of electro-thermal-mechanical effects. In this study, the electro-softening of the flow stress is defined as a stress drop. A possible internal mechanism is that the electrical current changes the interaction between dislocations, reduces the energy barrier of dislocation movement, and promotes dislocation slip [27]. When entering the pulse interval, the flow stress of the Al alloys increases sharply owing to the disappearance of the electrical current effect in the material, which exhibits remarkable strain hardening before the next cycle. In other words, the Al alloys complete a "stress drop-strain hardening" behavior within one pulse cycle. As the EAT continues, a ratchet shape stress–strain curve consisting of multiple "stress drop-stress hardening" cycles is obtained. Combining Fig. 4(a and b), the average surface temperature of the EAT specimens is only slightly higher than the RT. The effect of electrical current on the plasticity of the material cannot be simply attributed to the Joule heating effect, implying that the athermal effect of electrical current also has an important contribution to the plasticity of the Al alloys.

In the test, the stress drop caused by EAT increased with an increase in the true strain. When the EAT parameters were set to $J = 50$ A/mm^2, $t_d = 1$ s, $\omega = 10$ s, and $\dot{\varepsilon}_p = 0.003$ s^{-1} (as shown in Fig. 6(b)), AA 7075-T6 experienced a total of four stress changes. And the values of stress drop at true strains of 0.024, 0.051, 0.077, and 0.10 were 128.95,

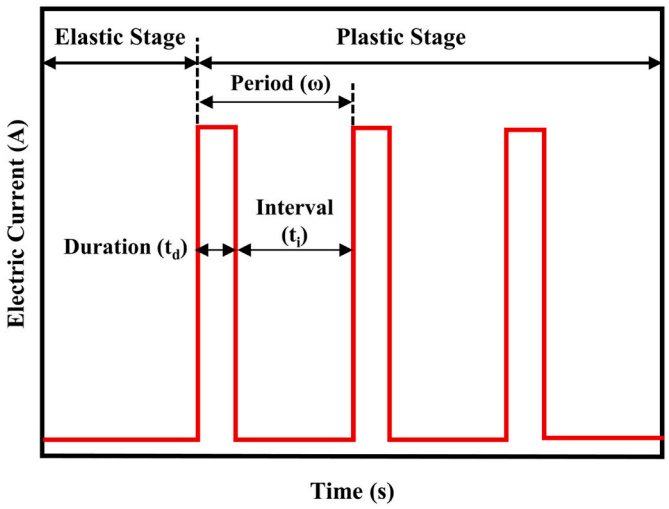

Fig. 3. Schematic diagram of pulsed electrical current waveform applied during EAT.

Table 2
Experiment parameters for EAT.

No.	Material	Electrical current density J (A/mm^2)	Pulse duration t_d (s)	Pulse period ω (s)	Strain rate $\dot{\varepsilon}_p$ (s^{-1})
1	AA 6061-T6	50	1	10	0.001
2					0.003
3					0.005
4				30	0.001
5					0.003
6					0.005
7	AA 7075-T6	50	1	10	0.001
8					0.003
9					0.005
10				30	0.001
11					0.003
12					0.005

226.00, 262.65 and 286.62 MPa, respectively, corresponding to each pulse period. This result may be attributed to the decrease in the cross-sectional area of the Al alloys during plastic deformation, which increased the real electrical current density, leading to an enhancement of the dislocation motion and the stress drop effect in the Al alloys. In addition, it can be seen from Fig. 5(a–c) and Fig. 6(a–c) that the phenomena of stress drop are more apparent when the strain rate is higher. Hence, during the EAT, the influence of the pulsed electrical current on the dislocation movement becomes more significant when the strain rate is higher.

The experimental results of Fig. 5(a–c) and 6(a-c) indicate that the true strain of the EAT specimen is lower than that of the NC specimen under the EAT parameters in these cases. However, a closer comparison of the above experimental results further reveals that the plasticity of the material can be improved to some extent by increasing the electrical current density or pulse duration, making it closer to or even much higher than the NC specimen. Generally, the plasticity of metals can be affected by the internal dislocations, second phase, grain size, and texture orientation of Al alloys caused by an external field during uni-directional tensile tests. In particular, existing findings suggest that the reduction of metal flow stress due to electrical current may originate from the important effect of electrical current on the process of internal dislocation evolution in metals under the combined electro-thermo-mechanical effects [48,49]. Therefore, an electroplasticity constitutive model of Al alloys based on the dislocation density evolution is introduced to describe the ratchet shape mechanical response of materials under the pulsed electrical current effect.

4. Basic theory of the constitutive model

In recent years, compared with phenomenological crystal plasticity constitutive models based on empirical formulas, crystal plasticity constitutive models based on physical micromechanism and the internal microstructure evolution of the material have received increasing research attention because of their higher accuracy. Kreyca and Kozeschnik [50] used thermal activation theory and the Kocks–Mecking dislocation evolution equation to describe the complex temperature- and strain-rate-dependent plastic deformation characteristics of Al–Mg alloys over a wide range of temperatures (78–650 K), strain rates (10^{-4}–10 s^{-1}), and solute contents (0–5 wt%). Wang et al. [51] used a power function of the acoustic energy density to correct the ejection work of dislocations from grain boundaries. And, the model could simulate the acoustic softening effect of the Hall–Petch slope under low-strain conditions. However, the effect of acoustic softening on the evolution of dislocation distribution was not considered, resulting in overestimations at high strains. Hunter and Preston [52] developed a model for the evolution of dislocation density in face-centered cubic (FCC) polycrystals considering dislocation generation, storage, and dynamic recovery. It was derived from the model in which the evolution and annihilation of moving dislocations in crystals are associated with the nucleation of grain boundaries. In addition, the mechanism of

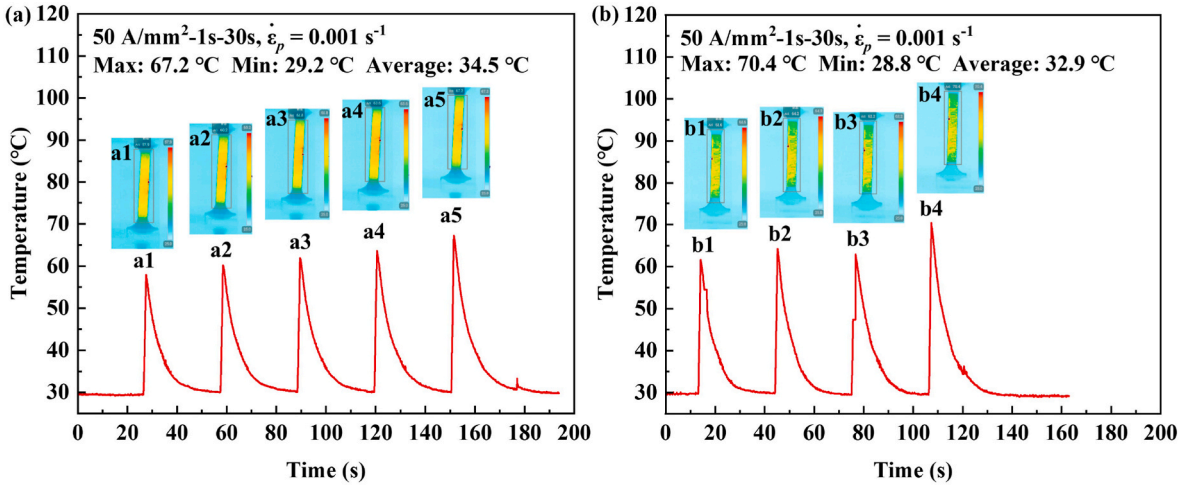

Fig. 4. Temperature test results of specimens during EAT: (a) AA 6061-T6; (b) AA 7075-T6.

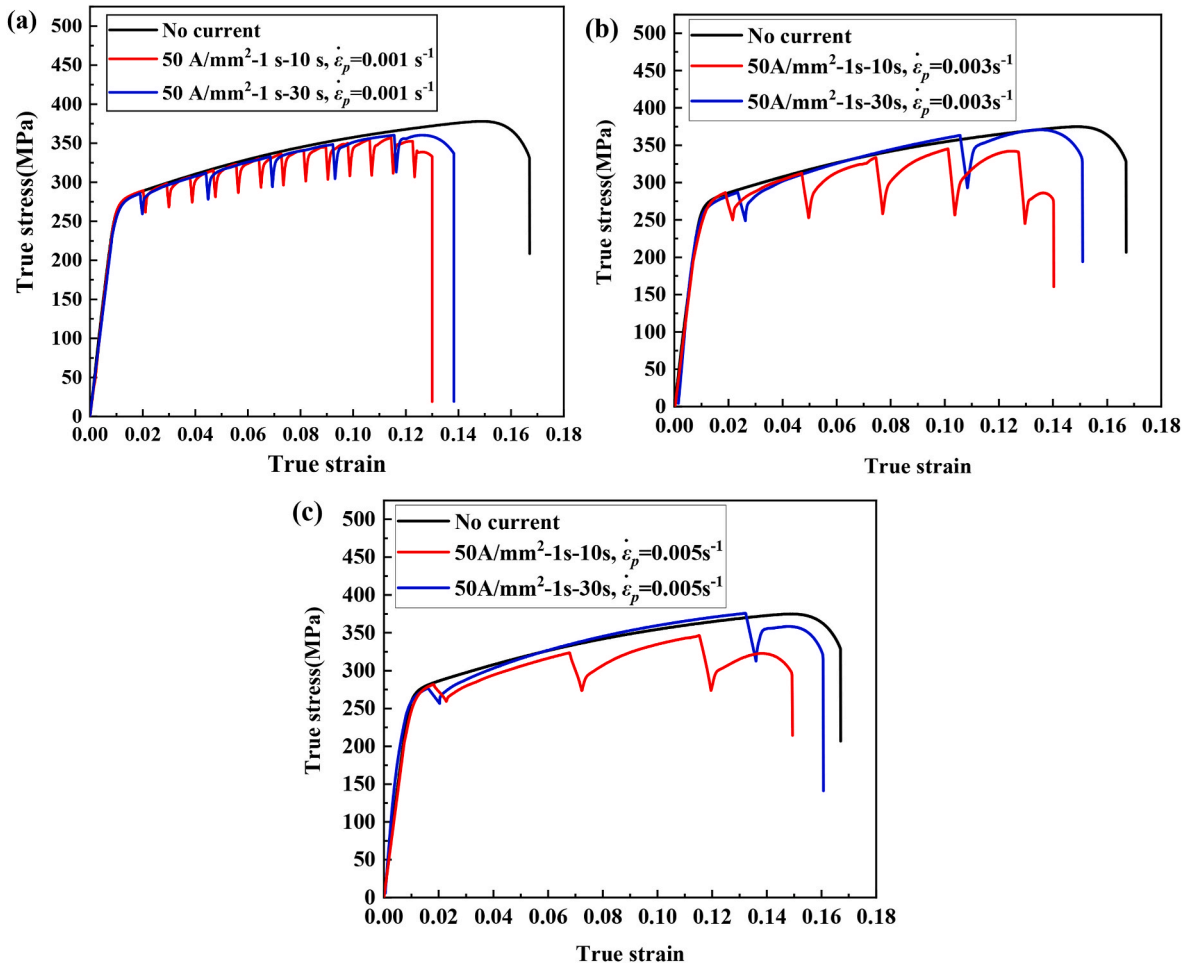

Fig. 5. Result of the EAT on the AA 6061-T6 under various parameters: (a) $J = 50$ A/mm^2, $t_d = 1$ s, $\dot{\varepsilon}_p = 0.001$ s^{-1}; (b) $J = 50$ A/mm^2, $t_d = 1$ s, $\dot{\varepsilon}_p = 0.003$ s^{-1}; (c) $J = 50$ A/mm^2, $t_d = 1$ s, $\dot{\varepsilon}_p = 0.005$ s^{-1}.

dislocation evolution has an explicit dependence on the density and temperature of the material. Gao et al. [42] established an electro-thermal-mechanical crystal plasticity model to simulate the thermal and athermal effects of pulsed electrical current assisted formation of superalloys. The results showed that the Joule heat is related to the direction of the applied electrical current and crystal defects, and the athermal effect of the electrical current can reduce the activation energy of dislocation slipping and accelerate the evolution rate of moving dislocations. Dislocation motion is primarily associated with thermal activation and stress driving. Therefore, a crystal plasticity framework based on the dislocation density and thermal activation theories can better reflect the dislocation evolution process during the plastic deformation of materials and accurately simulate the stress–-strain behavior. In this study, the metallic materials underwent coupled electrical-thermal-mechanical effects simultaneously during the EAT. And it can be preliminarily predicted that the parameters related to the stress variation and dislocation density evolution of the materials should be temperature-dependent. Thus, a framework for electroplasticity based on the dislocation density evolution and thermal activation theory was established. Among the various equations governing crystal plasticity, only those involved have been described.

Fig. 7 shows a flow chart for establishing an electroplasticity constitutive model. The basic idea is as follows: firstly, the constitutive relationship between the flow stress and plastic strain of materials under NC tension at RT is established based on the microscopic Taylor polycrystalline, thermal activation, and dislocation evolution models. Second, a single-parameter dislocation density electroplasticity constitutive model was established by modifying the material parameters according to electron wind theory. Finally, a two-parameter dislocation density electroplasticity constitutive model was developed by introducing forward and reverse dislocation densities to describe the strain-hardening behavior induced by the electron-dislocation non-equilibrium scattering effect and applied stress.

4.1. Establishment of the basic constitutive model

To obtain the relationship between stress and strain based on the microscopic slip mechanism of crystals, the relationship between the normal macroscopic stress–strain and shear stress–strain of the slip system was determined. The Taylor polycrystalline model is generally used to establish an approximately simplified relationship between the uniaxial stress–strain of a polycrystalline material and the shear stress–strain of a single crystal [53]:

$$M = \sigma / \tau = \gamma_p / \varepsilon_p \tag{1}$$

where M characterizes the Taylor factor, related to the texture evolution. In this study, M was determined to be constant ($M = 3.06$) [54] because the variation in M is small compared to the variation in the dislocation density. σ and ε_p are the flow stress and normal plastic strain, respectively. τ and γ_p are the critical shear stress and shear strain of the activated slip system, respectively.

The plastic deformation of metals at RT is mainly related to dislocation motion and the interaction between dislocations and obstacles

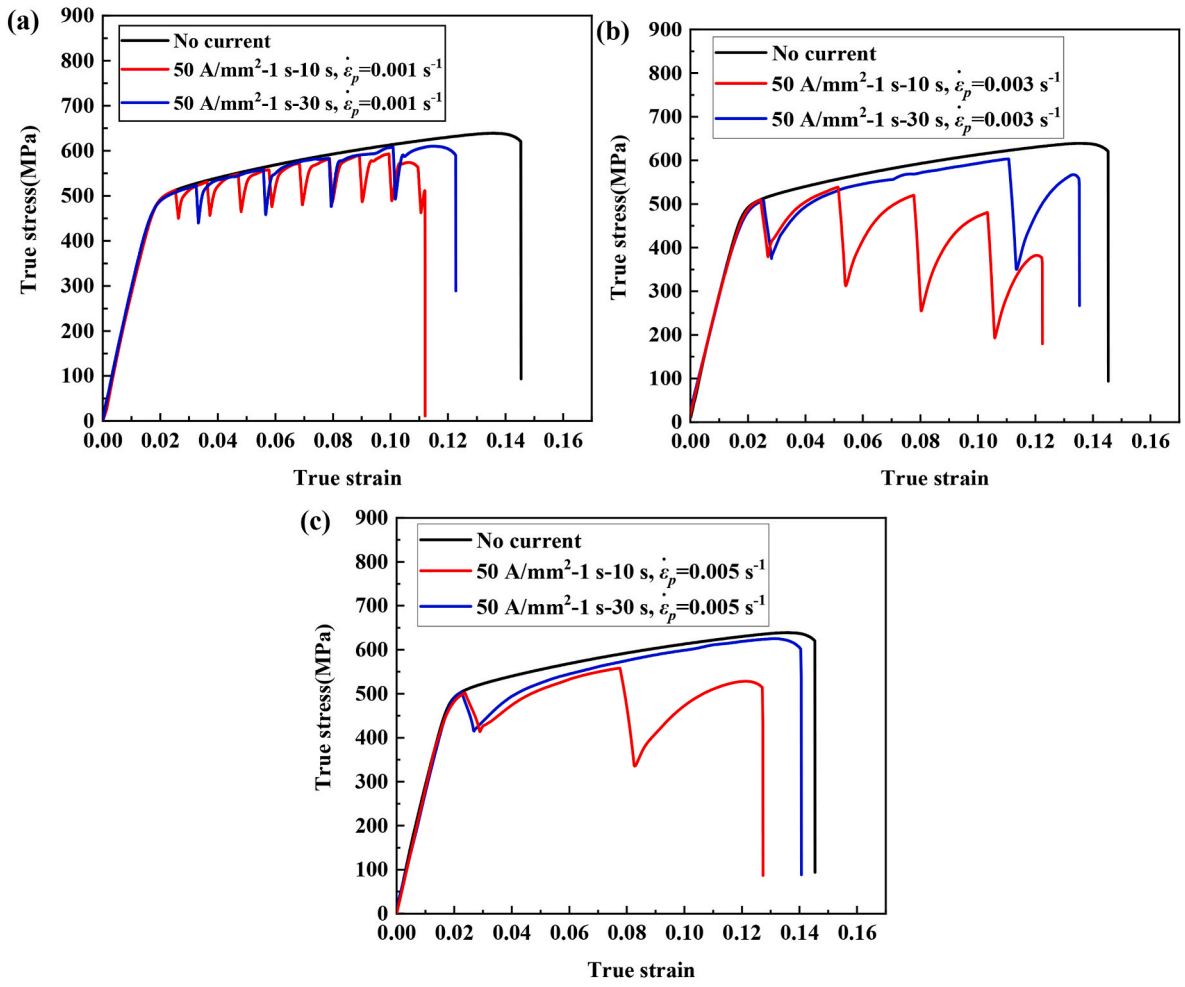

Fig. 6. Result of the EAT on the AA 7075-T6 under various parameters: (a) $J = 50$ A/mm^2, $t_d = 1$ s, $\dot{\varepsilon}_p = 0.001$ s^{-1}; (b) $J = 50$ A/mm^2, $t_d = 1$ s, $\dot{\varepsilon}_p = 0.003$ s^{-1}; (c) $J = 50$ A/mm^2, $t_d = 1$ s, $\dot{\varepsilon}_p = 0.005$ s^{-1}.

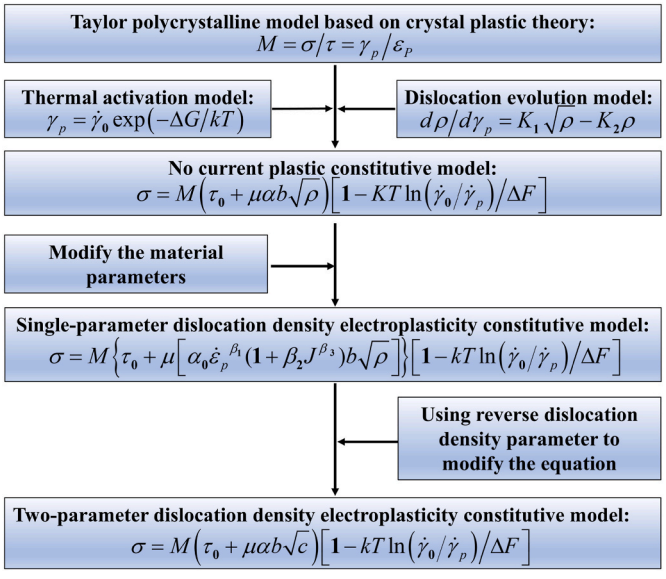

Fig. 7. Flow chart of electroplasticity constitutive modeling.

[55]. In addition to external loads, dislocations can overcome obstacles using thermal energy. Therefore, at the same strain rate, the flow stress of the material usually decreases as the temperature increases. This phenomenon can be explained using a thermal activation model. A commonly used thermal activation model is expressed using the Arrhenius equation [56]:

$$\dot{\gamma}_p = \dot{\gamma}_0 \exp\left(\frac{-\Delta G}{kT}\right) \tag{2}$$

where $\dot{\gamma}_p$ denotes the shear plastic strain rate, $\dot{\gamma}_0$ denotes the pre-exponential factor (or frequency factor), k denotes the Boltzmann constant, T denotes the thermodynamic temperature. ΔG denotes the activation-free enthalpy. Here, the strengthening second-phase η' or Guinier-Preston (GP) II zone in the investigated alloys are nanoscale and regarded as uniformly distributed in the Al matrix. Therefore, the interaction between the dislocations and the second phase can be considered to be short-range. For the activation-free enthalpy change of short-range obstacles, a simplified model suitable for various obstacle distribution forms has been proposed [56]:

$$\Delta G = \Delta F\left[1 - \left(\frac{\tau}{\hat{\tau}}\right)^p\right]^q \tag{3}$$

where ΔF is the total activation energy required for the dislocation to surmount the barrier, $\hat{\tau}$ is the mechanical threshold, considered the shear strength of the materials at 0 K. p and q are obstacle distribution parameters, with their range of $0 < p \leq 1$ and $1 \leq q \leq 2$. For simplicity, the values of p and q were assumed to be $p = q = 1$. A hypothetical value commonly used in other studies [55,57]. The mechanical threshold $\hat{\tau}$ depends on the dislocation density ρ, and their relationship reflects the

change in mechanical strength caused by the change in the dislocation density during the plastic deformation process. It was usually expressed as [58]:

$$\widehat{\tau} = \tau_0 + \mu\alpha b\sqrt{\rho} \tag{4}$$

where τ_0 is the friction stress, which is related to lattice friction and solute content. μ is the elastic shear modulus, α is a parameter related to the material and depends on temperature and strain rate. b is the length of the Burgers vector.

During plastic deformation, the slip and multiplication of dislocations located on the close-packed surface and in the close-packed direction led to drastic changes in the dislocation density of the material. So, the mechanical threshold and strength of the material was altered. The variation in dislocation density was the result of the combined effect of dislocation storage and dislocation recovery. A typical form of dislocation evolution theory is as follows [58]:

$$\frac{d\rho}{d\gamma_p} = K_1\sqrt{\rho} - K_2\rho \tag{5}$$

where the dislocation storage coefficient K_1 is regarded as a constant. And, the dynamic recovery coefficient K_2 depends on the plastic strain rate and temperature. It can be expressed as [59]:

$$K_2 = K_{20}\left(\frac{\dot{\varepsilon}_p}{\dot{\varepsilon}_0}\right)^{-1/n} \tag{6}$$

where K_{20} is a constant, $\dot{\varepsilon}_0$ and n are temperature-dependence parameters.

The integral of Eq. (5) can be obtained:

$$\sqrt{\rho} = \left(\sqrt{\rho_0} - \frac{K_1}{K_2}\right)\exp\left(-\frac{MK_2}{2}\varepsilon_p\right) + \frac{K_1}{K_2} \tag{7}$$

where ρ_0 is the initial dislocation density when the strain is zero.

By simultaneously considering Eqs. (1)–(7), the constitutive relationship between the flow stress σ and the plastic strain ε_p of the material under the NC condition, which is also the basic equation of the subsequent electroplasticity constitutive model. It can be expressed as:

$$\sigma = M\left(\tau_0 + \mu\alpha b\sqrt{\rho}\right)\left[1 - kT\ln\left(\dot{\gamma}_0 \Big/ \dot{\gamma}_p\right) \Big/ \Delta F\right] \tag{8}$$

4.2. Experimental verification of the basic constitutive equations

To verify the accuracy of the model (Eq. (8)), AA 6061-T6 and AA 7075-T6 were tested under NC conditions, respectively. And the predicted and experimental data were compared. The results of the NC tensile tests and the predictions based on Eq. (8) for AA 6061-T6 and AA 7075-T6 are shown in Fig. 8, respectively. Here, R is the correlation coefficient between the test and predicted results. R ranges from 0 to 1. The closer the R value is to 1, the higher the agreement between the two datasets. The correlation coefficient of the model predictions for the two Al alloys was 0.99. Obviously, the experimental results for NC tension are consistent with the predicted results based on Eq. (8).

5. Electroplasticity constitutive models of Al alloys

5.1. Single-parameter dislocation density electroplasticity constitutive model

5.1.1. Model establishment

Tests and theoretical studies have shown that electrical current significantly impacts the mechanical behavior of materials. In this study, a pulsed electrical current was applied during plastic deformation, resulting in an instantaneous reduction in the flow stress. According to the classical electron wind theory, drifting/moving electrons can transfer momentum to atoms, promoting the electromigration effect at the interface of the defect structure [60]. Moreover, electrons can induce atomic vibration at the dislocation, overcoming the Peierls energy barrier and promoting dislocation motion [34]. However, the results of Sprecher et al. [15] and Tiwari et al. [61] showed that the value of the electron wind force (F_{ew}) is approximately 0.1 MPa, which is insufficient to drive the dislocations for long-range motions. In addition, during EAT, the electrical current interacts with the non-uniformly distributed microstructure, which may lead to a non-uniform distribution of the internal temperature of the material. For example, Fan et al. [62] found that localized melting of the grain boundaries of brass alloys occurs when the overall temperature of the material is significantly lower than the melting point under the action of an electrical current field. Our recent results suggest that the non-equilibrium scattering of electron dislocations leads to an increase in the local temperature at the dislocations. It will form temperature gradients at the atomic scale and promote the cross-slip migration of screw dislocations [27,47]. The above results indicate that the thermal and athermal effects of the electrical current occur simultaneously when the electrical current interacts with the internal structure of the material and improve the mechanical properties under appropriate process parameters. It has been proven for pure Al, Al alloys, and other metals [22,46]. When an electrical current passes through the metal during the plastic deformation process, the electron wind force (F_{ew}, proportional to the electron drift speed) can promote dislocation motion. Based on experimental research on different materials, Conrad [63] proposed that the electrical current in the metal does not change the control mechanism of the strain rate,

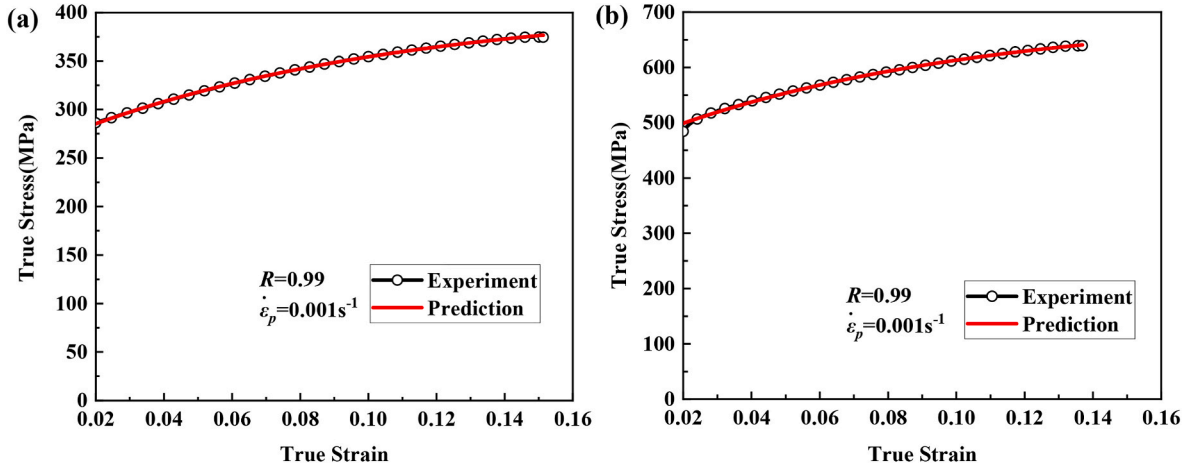

Fig. 8. Comparison between experimental and predicted results of three types of Al alloys: (a) AA 6061-T6; (b) AA 7075-T6.

but only affects the thermal component of the flowing stress in the direction of the electrical current. At high temperatures and low strain rates, the effect of the pulsed electrical current on plastic deformation is weakened [28], suggesting that the electrical current only affects the thermal component of the flow stress generated by short-range obstacles. Therefore, it is reasonable to modify the temperature-sensitive parameters (α and n) to couple the influence of electrical current density on the mechanical behavior of the materials [39,44]. In the EAT, the macroscopic peak temperature of the specimen can reach 154.8 °C, thus indicating that temperature affects the relevant material parameters.

The material parameter α depends on the strain rate and temperature. Since the temperature mainly comes from the Joule heat generated by the pulsed electrical current, the parameter α including the effects of strain rate, temperature and the pulsed electrical current is expressed by the following equation:

$$\alpha = \alpha_0 \dot{\varepsilon}_p^{\beta_1} \left(1 + \beta_2 J^{\beta_3}\right) \tag{9}$$

The material parameter n is also related to the deformation temperature. Similar to the parameter α, the parameter n can be expressed by the following equation:

$$n = \beta_4 T^{\beta_5} \left(1 + \beta_6 J^{\beta_7}\right) \tag{10}$$

where α_0 and β_1 in Eq. (9) were calculated from the results of the NC tensile tests at RT with different strain rates. β_4 and β_5 in Eq. (10) was calculated by fitting the results of the NC tensile tests at the same strain rate at different temperatures. β_2, β_3, β_6 and β_7 in Eqs. 9 and 10 were obtained by fitting the results of EAT with different electrical current densities. Among them, β_2, β_3, β_6 and β_7 are parameters related to the electrical current density (J) and used to describe the electroplasticity effect produced by the pulsed electrical current. It is generally related to the electron wind force. The material parameters α and n are varied by the applied pulsed electrical current density, highlighting the effect of the pulsed electrical current on the plastic deformation of the material. Moreover, during the EAT, the average surface temperature of the material is not much different from the RT, and the n value varies within a certain range.

Relevant experimental results have proven that a pulsed electrical current can effectively promote dislocation migration and reduce the dislocation density [64]. An increase in the full width at half maximum (FWHM) can reflect an increase in the internal dislocation density of a material under the same test conditions. Fig. 9(a) show the patterns of X-Ray Diffraction (XRD) for AA 7075-T6 in the NC and EAT specimens with 10% and 13% true strain, respectively. The parameters of EAT are 60 A/mm^2-1s–30s, and $\dot{\varepsilon}_p = 0.001$ s^{-1}, which is to verify the variation of the dislocation density inside the material under the action of pulsed electrical current. Among these, a true strain of 10% corresponds to the end moment of the pulsed electrical current duration, and a true strain of 13% corresponds to the end moment of the pulse electrical current interval. In addition, the NC specimens with a true strain of 10 % were compared with the pulsed electrical current specimens to reflect the changes in the FWHM and dislocation density over the duration of the pulsed electrical current. All the XRD diffraction peaks were fitted using the pseudo-Voigt function to measure the dislocation density changes within the material. The microcrystal size and average microstrain were obtained using the Williamson-Hall formula, as shown in Eq. (11).

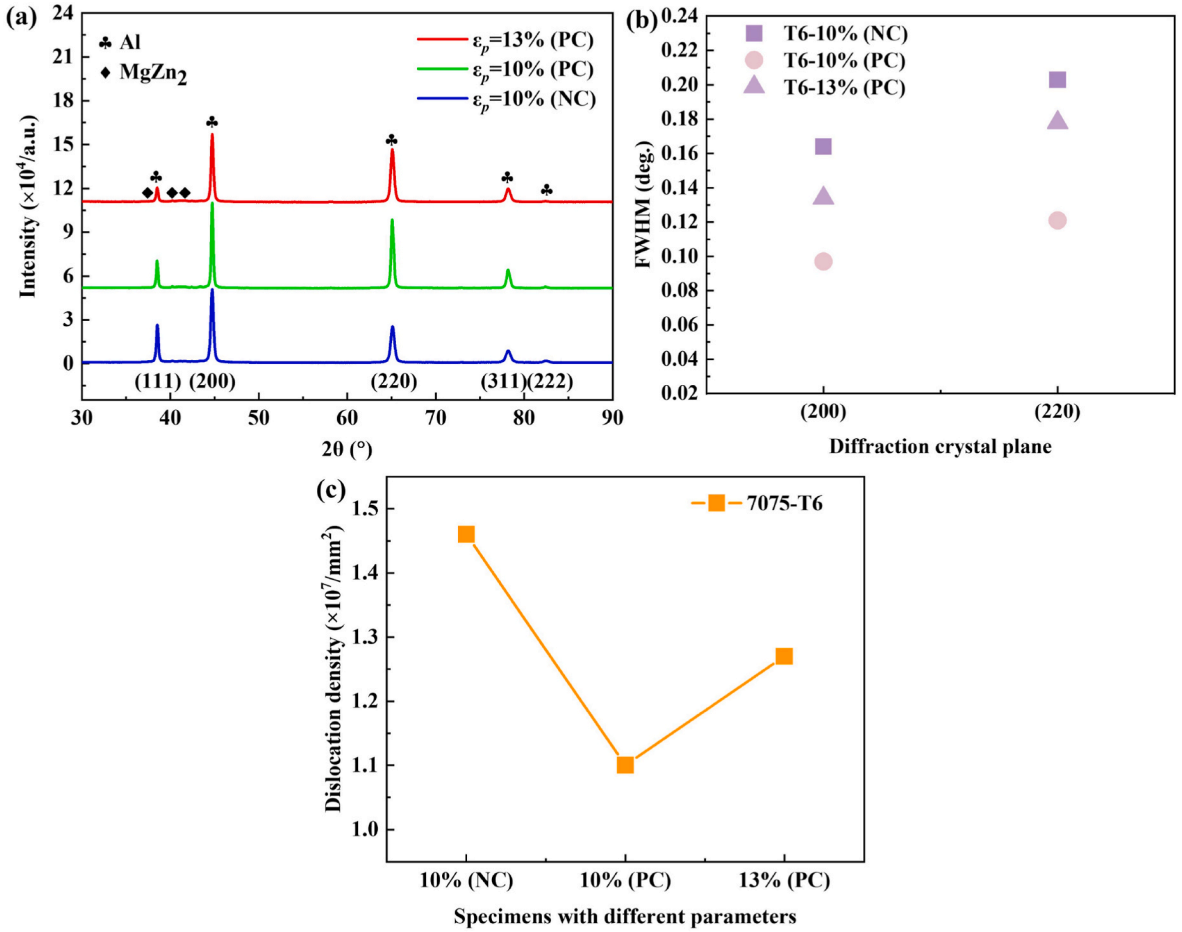

Fig. 9. XRD patterns and the dislocation density in AA 7075-T6: (a) XRD pattern for AA 7075-T6 (J = 60 A/mm^2, t_d = 2 s, ω = 30 s, $\dot{\varepsilon}_p$ = 0.001 s^{-1}); (b) FWHM profiles of the diffraction crystal plane; (c) dislocation density of different Al alloys.

Finally, the dislocation density was calculated using Eq. (12).

$$\beta \cos\theta = \frac{\lambda}{D} + 4\varepsilon_{micro} \sin\theta \tag{11}$$

$$\rho = \frac{2\sqrt{3}\varepsilon_{micro}}{Db} \tag{12}$$

where β is the FWHM, θ is the Bragg diffraction angle, λ is the diffraction wavelength of Cu K α, $\lambda = 0.154056$ nm, D is the average microcrystal size, ε_{micro} is the average microstrain. ρ is the dislocation density, and b is the Burgers vector length, $b = 2.86 \times 10^{-7}$ mm for Al alloys. Fig. 9(b) shows the statistical results for the FWHM values of the (200) and (220) crystal planes of AA 7075-T6 specimens. The AA 7075-T6 specimens presented the application of a pulsed electrical current caused a decrease in the FWHM value when the true strain was 10%, whereas the FWHM value increased again when entering the pulse interval period. Fig. 9(c) shows the dislocation densities calculated from the XRD data. The dislocation density trend was consistent with the FWHM, which indicates that the dislocation density in the material undergoes a reduction when the pulsed electrical current is applied. Based on the above results, a single-parameter dislocation density constitutive model of the electroplasticity was established:

$$\sigma = M\left\{\tau_0 + \mu\left[\alpha_0 \dot{\varepsilon}_p^{\beta_1}\left(1+\beta_2 J^{\beta_3}\right)\right] b\sqrt{\rho}\right\}\left[1 - kT\ln\left(\dot{\gamma}_0 \Big/ \dot{\gamma}_{\mathrm{p}}\right) \Big/ \Delta F\right] \tag{13}$$

5.1.2. Calculation of model parameters

The parameters in the above constitutive model were determined using MATLAB software by fitting the test data of the EAT (Figs. 5 and 6). And, these parameters are listed in Table 3. This constitutive model was used to predict the stress–strain behavior of Al alloys under EAT, with ($J \neq 0$) and without ($J = 0$) the electrical current density. At present, all the related parameters of the electroplasticity constitutive model with a single-parameter dislocation density have been determined. Notably, only the plastic deformation behavior of the material was considered, with the elastic deformation stage ignored. Therefore, the initial state for the numerical calculation was the yield point of the material.

(c) Experimental verification.

The experimental data of EAT (No. 7 in Table 2) were used to verify the single-parameter dislocation density electroplasticity constitutive model established above. Only a single pulse was used for verification. A schematic of the single pulsed electrical current waveform is shown in Fig. 10(a). And the true stress–true strain curve obtained from a single pulsed electrical current assisted quasi-static unidirectional tensile test is shown in Fig. 10(b). The true stress–true strain curves from experiment were compared with the predicted ones using the electroplasticity constitutive model (Eq. (13)), as shown in Fig. 10(b). The constitutive model can accurately predict the instantaneous stress drop of AA 7075-T6 when a pulsed electrical current is applied. However, there is a significant error in predicting the strain-hardening behavior during the pulsed electrical current interval. The predicted results indicates that the true stress of the material increases instantly to a level similar to the initial true stress–true strain when the pulsed electrical current enters the interval. A similar situation occurred for AA 6061-T6. Therefore, the above constitutive model needs to be further modified to accurately predict the strain-hardening behavior of the material during the pulse interval.

5.2. Two-parameter dislocation density electroplasticity constitutive model

5.2.1. Model establishment

When the material is subjected to periodic coupling effects of electrical-thermal-mechanical, it exhibits complex electroplastic behavior. An instantaneous decrease in the flow stress of the material occurred during the continuous action of the electrical current. When entering the pulse interval, the flow stress of the material increased with increasing strain. It means that materials exhibit periodic electro-softening and strain-hardening behaviors during EAT. As mentioned above, the two-parameter dislocation density model proposed by Rauch et al. [43] can predict the Bauschinger effect and evolution law of the dislocation density of the material, which is the periodic effects under external cyclic loading. In fact, when a pulsed electrical current is applied, the periodic ratchet shape mechanical response behavior of the material can be also considered using a similar descriptive method due to the periodic turn-on and turn-off of the electrical current. In this section, the two-parameter dislocation density model is mainly used to modify Eq. (13) so that the predicted results are as consistent as possible with the experimental results.

When the electrical current interacts with the atoms inside the material, it can introduce electrostatic forces between the atoms by charge transfer, which can affect the microstructural evolution [65]. Li et al. [8] revealed that dislocations inside a material can undergo reciprocating motion controlled by an electrical field. Our recent results showed that the effect of electrical current on material properties is not only reflected in the simultaneous action of electrical-thermal-mechanical effects, but also in the asynchronous effects of pre-deformation and pulsed electrical current [27]. After the material is subjected to a pulsed electrical current treatment, the internal screw dislocations are more prone to cross-slip [26] under the action of the non-equilibrium scattering of electron dislocations. This will promote the generation of edge dislocations and leads to an increase in dislocation density [27]. For EAT, when the material enters the pulse interval, the material is equivalent to an asynchronous electrical–mechanical treatment, as described above. Therefore, dislocation accumulation in the material during the pulse interval is the result of the combined effect of electron-dislocation non-equilibrium scattering and applied stresses. This effect can be regulated by reverse dislocation density. As the strain increased, the reverse dislocation density gradually decreased to zero according to a specific evolutionary law.

The change in the mechanical behavior of materials shows that the electroplastic behavior has apparent directionality when a pulsed electrical current is applied. The reduction of stress owing to the application of electrical current depends on the direction of the electrical current [66]. When the flow direction of the drifting electrons is the same as that of the applied force, the electrons generate a positive electron wind force (F_{ew}^{+}) for mobile dislocations. When the flow direction of the drifting electrons is opposite to that of the applied force, the electrons generate a negative electron wind force (F_{ew}^{-}) for mobile dislocations. The reverse dislocation density can be used to modify the evolution of the dislocation density in a material when the electrical current polarity is reversed. In the EAT, each pulse cycle was divided into two stages: pulse duration and pulse interval. The instantaneous stress-drop behavior of the material during the pulse duration can be depicted using an electroplasticity constitutive model with a single-parameter dislocation density (Eq. (13)). In the pulse interval, the total dislocation density is divided

Table 3
Parameter values of the electroplasticity constitutive model with single-parameter dislocation density for AA 7075-T6.

M	K (J/K)	τ_0 (MPa)	μ (MPa)	$\dot{\gamma}_0$ (s^{-1})	$\dot{\gamma}_p$ (s^{-1})	α_0	K_1	K_{20}	
3.06	$1.38e^{-23}$	30.67	27000	10^6	$\sqrt{3}\dot{\varepsilon}$	0.55	698556.49	39.26	
ρ_0 (mm^{-2})	b(mm)	$\dot{\varepsilon}_0$ (s^{-1})	β_1	β_2	β_3	β_4	β_5	β_6	β_7
4.04×10^9	2.86×10^{-7}	1.54×10^{-7}	0.0665	−0.005	0.7	0.15	0.6149	0.007	0.85

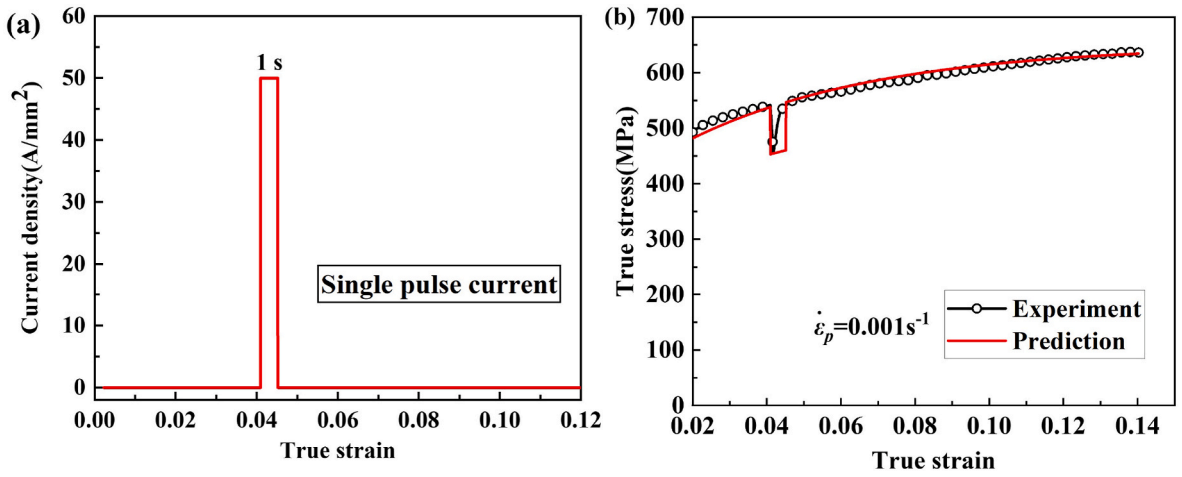

Fig. 10. AA 7075-T6 sheet undergoing a single pulse during the EAT: (a) schematic diagram of single pulsed electrical current waveform; (b) comparison between the test and predicted results based on the electroplasticity constitutive model with single-parameter dislocation density.

into two parts: forward dislocation density (ρ_f)and reverse dislocation density (ρ_r).

Fig. 11(a–e) show a schematic diagram of the variation in the forward and reverse dislocation densities in the material during EAT. Fig. 11(a–e) correspond to points A–E in Fig. 11(f). In the duration stage of the EAT, the direction of motion of the electrons inside the material was consistent with the direction of the applied stress. At this time, there are mainly forward dislocation densities within the material, and the reverse dislocation density is zero, as shown in Fig. 11 (a). At the initial moment of the EAT interval stage, the direction of the electron motion is opposite to that of the applied stress because of the reversal of the electrical current polarity. At this point, part of the forward dislocation densities inside the material are transformed into reverse dislocation densities, as shown in Fig. 11(b). During the interval of the EAT, the reverse dislocation density inside the material decreased as the strain increased, as shown in Fig. 11(c). When the material was at the end of

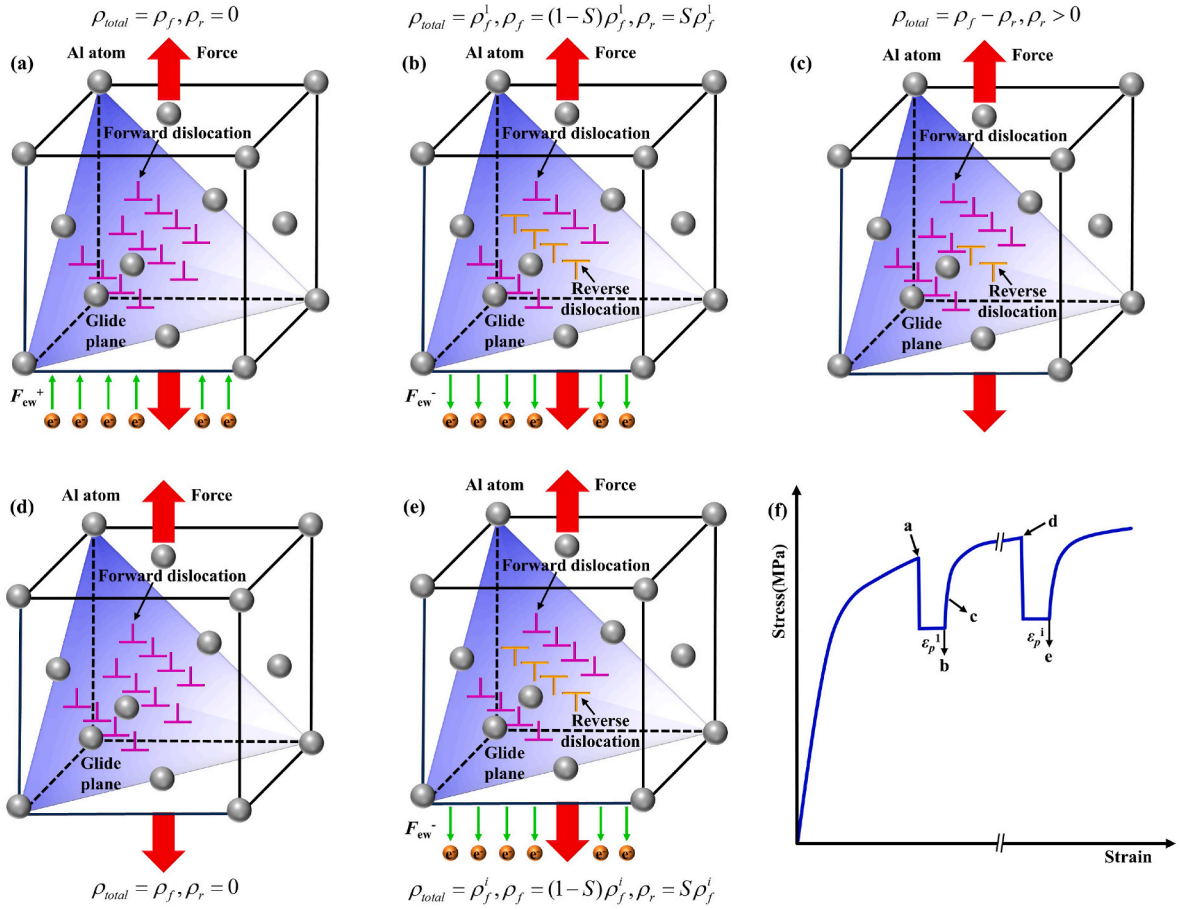

Fig. 11. Schematic diagram of the variations in the forward and reverse dislocation densities within the material during various stage of EAT: (a) initial moments of the EAT duration stage; (b) initial moments of the EAT interval stage; (c) middle moments of the EAT interval stage; (d) terminal moments of the EAT interval stage; (e) initial moment of the *i-th* EAT interval stage; (f) schematic diagram of stress–strain curve during EAT.

the EAT interval, the reverse dislocation density in the material decreased to 0. At this moment, the material enters the initial stage of the next EAT duration, as shown in Fig. 11(d). When the material was at the initial moment of the EAT interval stage of the *i-th* pulse cycle, the true strain corresponding to the tensile specimen was $\varepsilon_p{}^i$. The total dislocation density at this moment was ρ_f^i. When the strain is equal to $\varepsilon_p{}^i$, the total dislocation density is divided into two parts, i.e., $\rho_f(\varepsilon_p{}^i)$ and $\rho_r(\varepsilon_p{}^i)$. As shown in Fig. 11(e), the forward dislocation density and the reverse dislocation density can be calculated by Eqs. 14 and 15. During the EAT interval, the reverse dislocation density offsets the forward dislocation density. Thus, the total dislocation density is equal to the forward dislocation density minus the reverse dislocation density, that is $\rho_{total} = \rho_f - \rho_r$.

$$\rho_f(\varepsilon_p{}^i) = (1-S)\rho_f^i \tag{14}$$

$$\rho_r(\varepsilon_p{}^i) = S\rho_f^i \tag{15}$$

where S is a scalar quantity representing the percentage of the forward dislocation density converted to the reverse dislocation density when the electrical current ends.

The percentage of the total dislocation density converted to the reverse dislocation density was determined by the value of S. When $S = 0$, there is no reverse dislocation density at the end of the EAT. Therefore, the predicted stress–strain result is similar to that shown in Fig. 10. When $S > 0$, strain hardening began to appear. And as the value of S increased, the hardening characteristics also improved. When undergoing a single pulse, its true stress–true strain curves predicted by the two-parameter dislocation density electroplasticity constitutive model with different values of S are presented in Fig. 12(a).

The forward dislocation density evolution law is also given by Eq. (5). The evolution law of the reverse dislocation density follows the equation [44]:

$$\frac{d\rho_r}{d\varepsilon_p} = -HMK_1\sqrt{\rho_f}\,\frac{\rho_r}{\rho_f^i} \tag{16}$$

where H denotes a scalar representing the evolution rate of the reverse dislocation density.

The value of H in Eq. (16) determines the rate of evolution of the reverse dislocation density. The larger the value of H, the faster the evolution rate of the reverse dislocation density with strain. When undergoing a single pulse during EAT, the true stress-true strain curves predicted by the two-parameter dislocation density electroplasticity constitutive model with different values of H are exhibited in Fig. 12(b).

Since the reverse dislocation density can offset the forward dislocation density, the total dislocation density is reduced. Therefore, the flow stress of the material in the EAT interval is less than that in the NC tensile test. In the two-parameter dislocation density model, $\rho_f - \rho_r$ is used instead of ρ. Thus, the modified two-parameter dislocation density electroplasticity constitutive model can be expressed as follows:

$$\sigma = M\left[\tau_0 + \mu\left(\alpha_0\dot{\varepsilon}_p{}^{\beta_1}\right)b\sqrt{\rho_f - \rho_r}\right]\left[1 - kT\ln\left(\dot{\gamma}_0 \Big/ \dot{\gamma}_p\right) \Big/ \Delta F\right] \tag{17}$$

During EAT interval, the total dislocation density was divided into forward and reverse dislocation densities. At this stage, the stress–strain behavior of the material was consistent with the prediction of the two-parameter dislocation density electroplasticity constitutive model. At the second stage, the reverse dislocation density remained at zero, and the forward dislocation density was equal to the total dislocation density. That is, the stress–strain behavior of the material in this stage followed the single-parameter dislocation density electroplasticity constitutive model. Therefore, the stress–strain expression at different stages during EAT can be uniformly expressed as follows:

$$\sigma = M\left(\tau_0 + \mu ab\sqrt{c}\right)\left[1 - kT\ln\left(\dot{\gamma}_0 \Big/ \dot{\gamma}_p\right) \Big/ \Delta F\right] \tag{18}$$

where $a = \alpha_0\dot{\varepsilon}_p{}^{\beta_1}\left(1 + \beta_2 J^{\beta_3}\right)$, $c = \rho_f - \rho_r$, when the material is in the EAT duration stage, i.e., $J \neq 0$, $\rho_r = 0$. Then, $a = \alpha_0\dot{\varepsilon}_p{}^{\beta_1}\left(1 + \beta_2 J^{\beta_3}\right)$, and $c = \rho_f$. The calculation is performed using Eq. (13). When the material is in the EAT interval stage, i.e., $J = 0$, $\rho_r \neq 0$. Then, $a = \alpha_0\dot{\varepsilon}_p{}^{\beta_1}$, and $c = \rho_f - \rho_r$. The calculation is performed using Eq. (17).

Based on the above applicable conditions of the two-parameter electroplasticity constitutive model (Eq. (18)), a subroutine that can be used for the operation was established using MATLAB software. A flowchart of the numerical calculation procedure for the EAT model is shown in Fig. 13. And, the procedure is summarized as follows.

- Values were assigned to the variables to be used in EAT process.
- Read the true strain and temperature-time data recorded in real time, and the total time (t_{total}) used throughout EAT process was obtained.
- Divide t_{total} into three parts: the time experienced without pulsed electrical current (t_1), the EAT duration time (t_d), and the EAT interval time (t_i). That is $t_{total} = t_1 + t_d + t_i$. Among them, $t_1 \in [0, t_{apply}]$; $t_d \in [t_{apply} + (N-1)T, t_{apply} + x + (N-1)T]$; $t_2 \in [t_{apply} + x + (N-1)T, t_{apply} + NT]$, the $N \geqq 0$. Where t_1, t_d, and t_i are vectors that represent the total time of their respective time periods. t_{apply} denotes the moment of the first application of the electrical current. N represents the number of times the electrical current, and the T stands

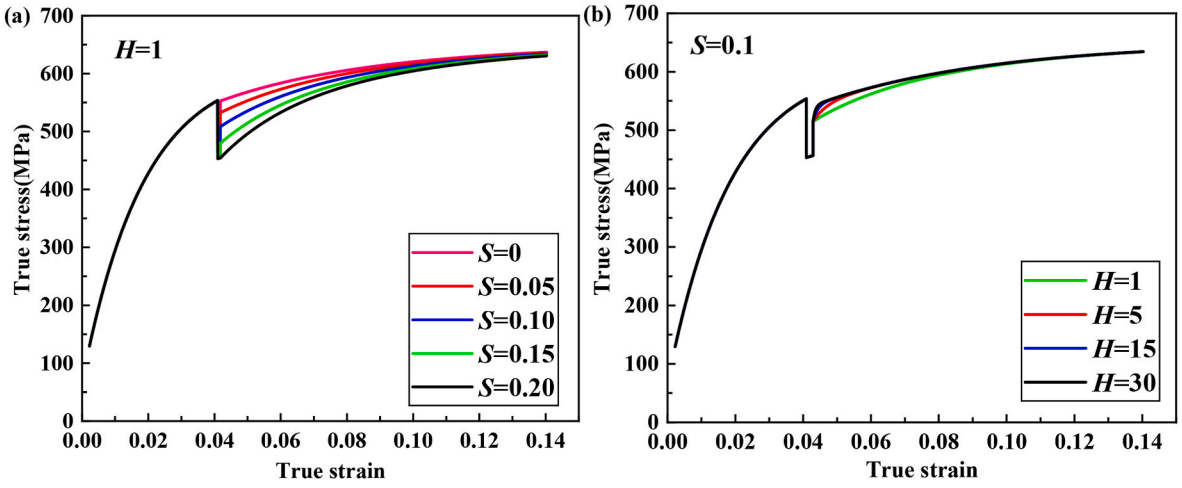

Fig. 12. Predicted true stress–true strain curve based on the two-parameter dislocation density electroplasticity constitutive model with (a) different values of S and (b) different values of H.

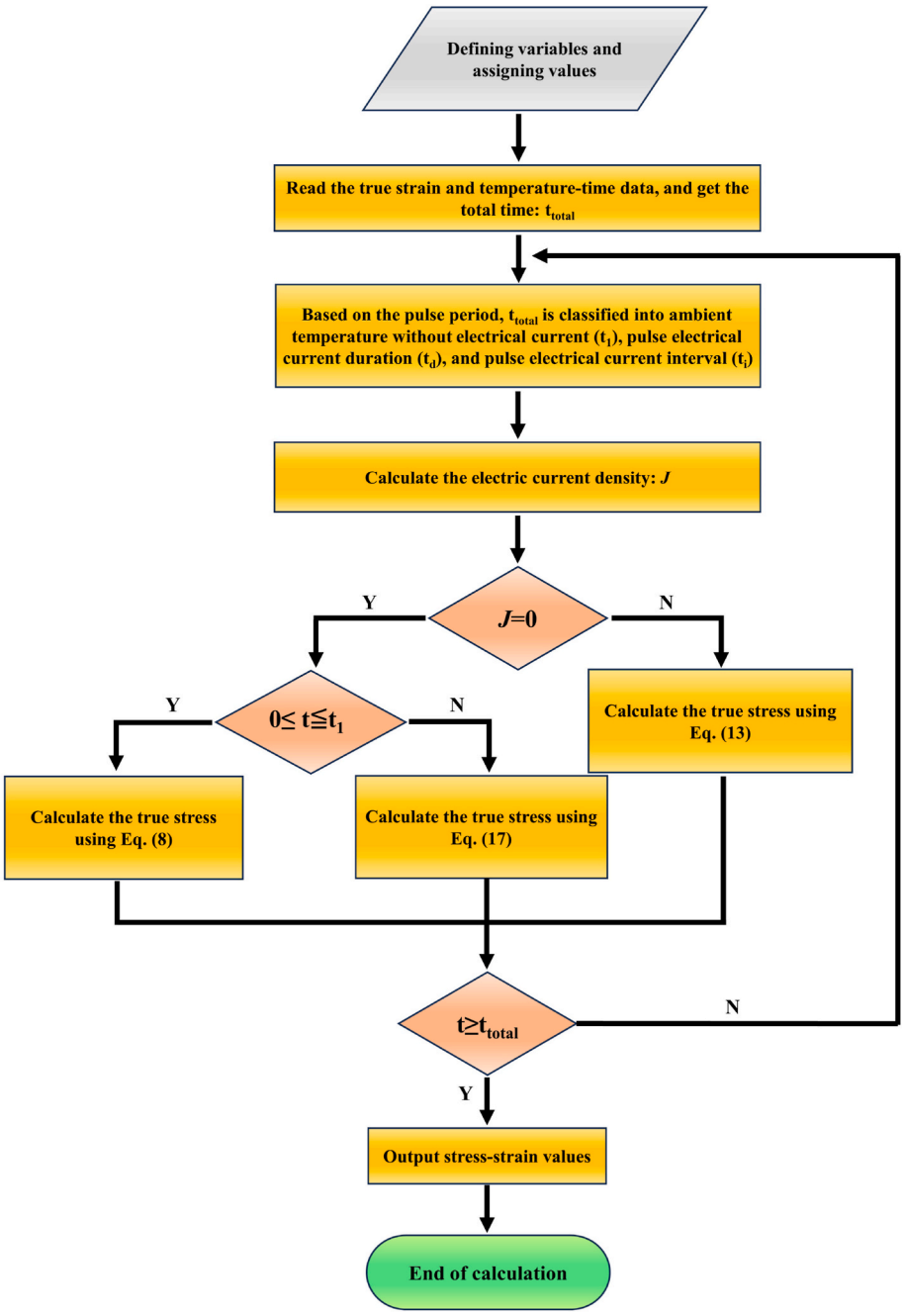

Fig. 13. Flowchart of the numerical calculation procedure of the electroplasticity constitutive model with two-parameter dislocation density.

for the pulse period. x is a variable that changes with the period, which represents the EAT duration.

- Calculate the electrical current density value J.
- Run Eq. (8) during NC assisted quasi-static unidirectional tension. Run Eq. (13) in the EAT duration stage. Run Eq. (17) in the EAT interval stage.
- The updated variable (t) is returned to the main routine of the electroplasticity constitutive model for the next calculation.
- Output the true stress values, and end this calculation.

5.2.2. Calculation of model parameters

Section 4.1 established the basic equation of the constitutive model based on crystal plastic mechanics. That is, the constitutive model between the flow stress and plastic strain in the NC tensile test (Eq. (8)). The Taylor factor (M), burgers vector length (b), pre-exponential factor ($\dot{\gamma}_0$), and total activation energy (ΔF) in this model are calculated by referring to the literatures [67,68]. The lattice resistance (τ_0) and the shear elastic modulus (μ) are calculated by fitting the data of the NC tensile tests. The material parameter (α) in Eq. (9) is a function of the strain rate ($\dot{\varepsilon}_p$) and electrical current density (J). Based on the above method, the parameter values of the two-parameter dislocation density electroplasticity constitutive models of AA 6061-T6 and AA 7075-T6 are listed in Tables 4 and 5.

5.2.3. Experimental verification

As mentioned above, the EAT results under different process parameters for AA 6061-T6 and AA 7075-T6 (in Table 2) were used to verify the two-parameter dislocation density electroplasticity constitutive model. The true stress–strain curves of the different alloys predicted by the constitutive model were compared with the test results obtained

Table 4
Parameter values of the two-parameter dislocation density electroplasticity constitutive model of AA 6061-T6.

M	K (J/K)	τ_0 (MPa)	μ (MPa)	$\dot{\gamma}_0$ (s^{-1})	$\dot{\gamma}_p$ (s^{-1})	α_0	K_1	K_{20}	ρ_0 (mm^{-2})	
3.06	$1.38e^{-23}$	1.17	27000	10^6	$\sqrt{3}\dot{\varepsilon}$	0.55	524490.94	39.21	2.44×10^9	
b (mm)	$\dot{\varepsilon}_0$ (s^{-1})	β_1	β_2	β_3	β_4	β_5	β_6	β_7	S	H
2.86×10^{-7}	1.54×10^{-7}	0.0665	−0.014	0.7	0.15	0.6149	0.047	0.1	0.11	23

Table 5
Parameter values of the two-parameter dislocation density electroplasticity constitutive model of AA 7075-T6.

M	K (J/K)	τ_0 (MPa)	M (MPa)	$\dot{\gamma}_0$ (s^{-1})	$\dot{\gamma}_p$ (s^{-1})	α_0	K_1	K_{20}	ρ_0 (mm^{-2})	
3.06	$1.38e^{-23}$	30.67	27000	10^6	$\sqrt{3}\dot{\varepsilon}$	0.55	698556.49	39.26	4.04×10^9	
b(mm)	$\dot{\varepsilon}_0$ (s^{-1})	β_1	β_2	β_3	β_4	β_5	β_6	β_7	S	H
2.86×10^{-7}	1.54×10^{-7}	0.0665	−0.005	0.7	0.15	0.6149	0.007	0.85	0.11	18

by EAT, as shown in Figs. 14 and 15, respectively. The correlation coefficient (R), average relative error (*AARE*) and root mean square error (*RMSE*) are used in the figure to represent the degree of agreement between the test and predicted results. The correlation coefficient R represents the linear relationship between the test and predicted results. The *AARE* and *RMSE* were calculated by comparing relative errors. Hence, unbiased statistical parameters were used to evaluate the model predictability. According to the definition of each evaluation index, $0 < R < 1$, the closer the R value is to 1, and the smaller the *AARE* and *RMSE* values, the higher the coincidence between the test results and the predicted results. Thus, the prediction results of the two-parameter dislocation density electroplasticity constitutive model and the experimental results are in good agreement. As the constitutive model of electroplasticity for EAT developed in this study is based on a physical mechanism, the constitutive model is expected to be applicable to most age-hardening alloys materials.

6. Conclusions

(1) The mechanical response behaviors of AA 6061-T6 and AA 7075-T6 in the electrical current assisted quasi-static unidirectional tension (EAT) were studied. During the EAT duration time, the

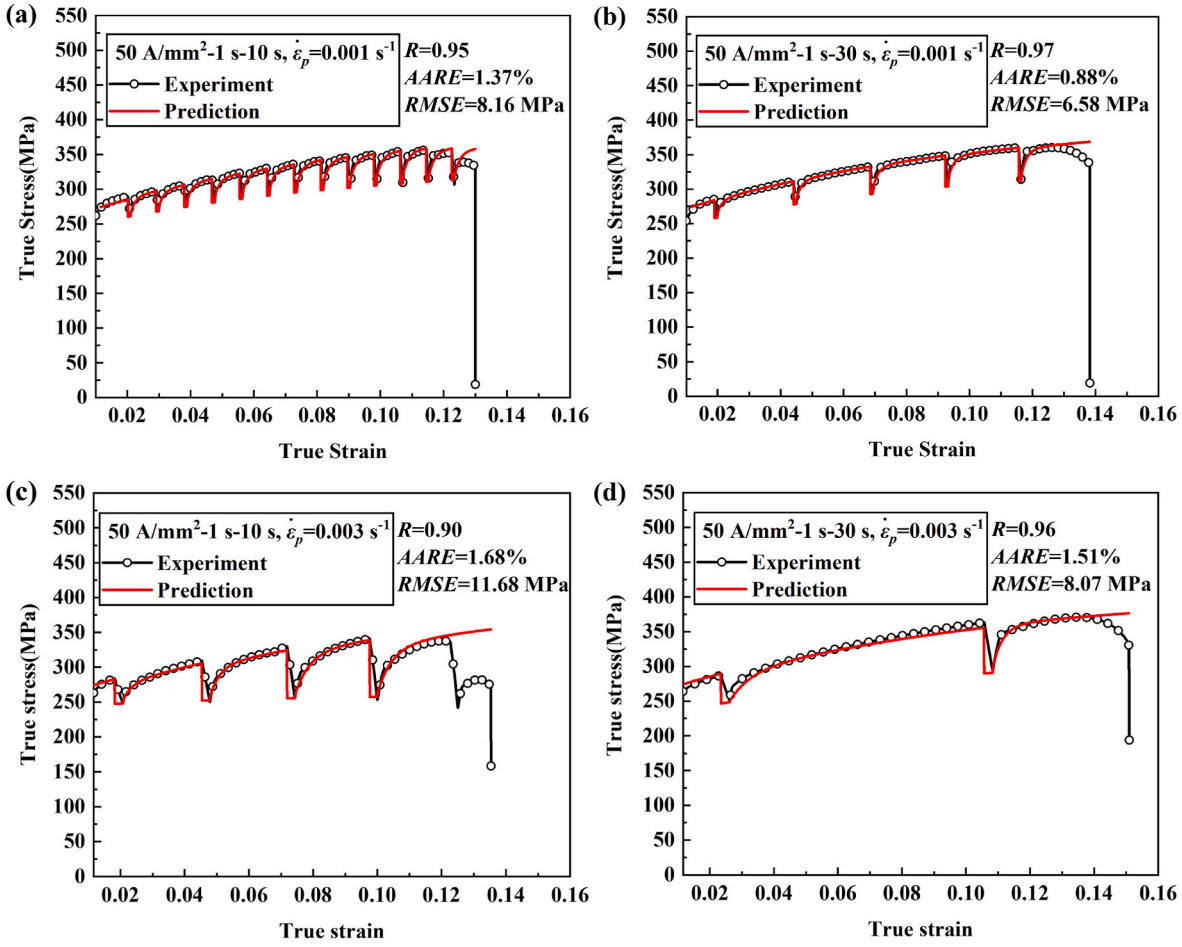

Fig. 14. Comparison of the experimental results and the predicted ones of the two-parameter dislocation density electroplasticity constitutive model for AA 6061-T6 sheet under various EAT parameters: (a) $J = 50$ A/mm^2, $t_d = 1$ s, $\omega = 10$ s, $\dot{\varepsilon}_p = 0.001$ s^{-1}; (b) $J = 50$ A/mm^2, $t_d = 1$ s, $\omega = 30$ s, $\dot{\varepsilon}_p = 0.001$ s^{-1}; (c) $J = 50$ A/mm^2, $t_d = 1$ s, $\omega = 10$ s, $\dot{\varepsilon}_p = 0.003$ s^{-1}; (d) $J = 50$ A/mm^2, $t_d = 1$ s, $\omega = 30$ s, $\dot{\varepsilon}_p = 0.003$ s^{-1}.

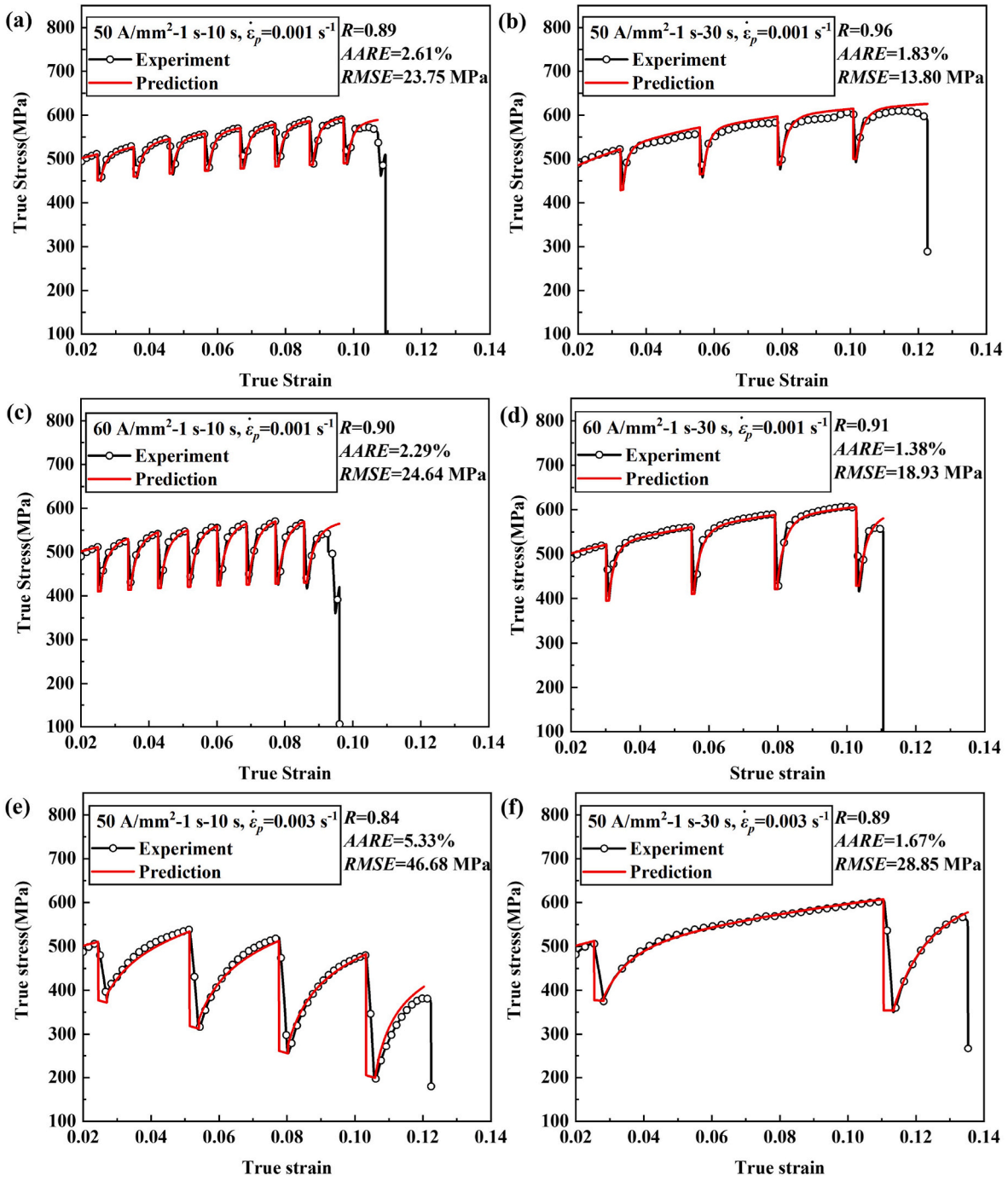

Fig. 15. Comparison of the experimental results and the predicted ones of the two-parameter dislocation density electroplasticity constitutive model for AA 7075-T6 sheet under various EAT parameters: (a) $J = 50$ A/mm^2, $t_d = 1$ s, $\omega = 10$ s, $\dot{\varepsilon}_p = 0.001$ s^{-1}; (b) $J = 50$ A/mm^2, $t_d = 1$ s, $\omega = 30$ s, $\dot{\varepsilon}_p = 0.001$ s^{-1}; (c) $J = 60$ A/mm^2, $t_d = 1$ s, $\omega = 10$ s, $\dot{\varepsilon}_p = 0.001$ s^{-1}; (d) $J = 60$ A/mm^2, $t_d = 1$ s, $\omega = 30$ s, $\dot{\varepsilon}_p = 0.001$ s^{-1}; (e) $J = 50$ A/mm^2, $t_d = 1$ s, $\omega = 10$ s, $\dot{\varepsilon}_p = 0.003$ s^{-1}; (f) $J = 50$ A/mm^2, $t_d = 1$ s, $\omega = 30$ s, $\dot{\varepsilon}_p = 0.003$ s^{-1}.

flow stress dropped immediately, whereas the material exhibited evident work hardening during the EAT interval time. The true stress–strain curve exhibited a unique periodic ratchet shape. The mechanical properties of materials are closely related to the parameters of the EAT.

(2) A two-parameter dislocation density model was developed based on the microscopic Taylor polycrystalline model, thermal activation theory, and dislocation density theory. In this model, the interaction between the dislocation and the second phase is approximated as short-range, which is more realistic than the long-range assumption in existing models. The parameters of the dislocation density constitutive model were determined, with a subroutine for the calculation was established using MATLAB software.

(3) The proposed electroplasticity constitutive model based on the forward and reverse dislocation density evolution can accurately predict the plastic deformation behavior of AA 6061-T6 and AA 7075-T6 sheets under the EAT, with the correlation coefficient R of 0.84–0.99 and the average relative error *AARE* less than 5.33%.

Data availability

Data will be made available on request.

CRediT authorship contribution statement

Yanli Song: Conceptualization, Methodology, Validation, Investigation, Data curation, Funding acquisition, Project administration. **Long Chen:** Funding acquisition, Writing – original draft, Writing – review & editing. **Chuanchuan Hao:** Methodology, Formal analysis, Data curation. **Lin Hua:** Investigation, Project administration, Resources. **Hainan Xu:** Formal analysis, Investigation. **Jue Lu:** Conceptualization, Resources, Methodology, Writing – review & editing. **Zhongmei Wang:** Formal analysis. **Jianguo Lin:** Formal analysis, Conceptualization. **Yanxiong Liu:** Formal analysis. **Lechun Xie:** Conceptualization, Formal analysis.

Declaration of competing interest

The authors declare that they have no known competing financial interests or personal relationships that could have appeared to influence the work reported in this paper.

Acknowledgements

This work was financially supported by the National Key R&D Program of China (No. 2020YFA0714900), the National Natural Science Foundation of China (Grant No. 51975440), Hubei Provincial "Chutian Talent Plan" Science and Technology Innovation Team, the Fundamental Research Funds for the Central Universities (WUT:2023III002JL, WUT:2023IVB060 and WUT: 104972024JYS0033).

References

[1] Lu J, Song YL, Hua L, Zheng KL, Dai DG. Thermal deformation behavior and processing maps of 7075 aluminum alloy sheet based on isothermal uniaxial tensile tests. J. Alloy. Compd. 2018;767:856–69. https://doi.org/10.1016/j.jallcom.2018.07.173.

[2] Ku AY, Khan AS, Gnäupel-Herold T. Quasi-static and dynamic response, and texture evolution of two overaged Al 7056 alloy plates in T761 and T721 tempers: experiments and modeling. Int J Plast 2020;130:102679. https://doi.org/10.1016/j.ijplas.2020.102679.

[3] Choi Y, Lee J, Panicker SS, Jin H, Panda SK, Lee M. Mechanical properties, springback, and formability of W-temper and peak aged 7075 aluminum alloy sheets: experiments and modeling. Inter. J. Mech. Sci. 2020;170:105344. https://doi.org/10.1016/j.ijmecsci.2019.105344.

[4] Rong Q, Shi ZS, Li Y, Lin JG. Constitutive modelling and its application to stress-relaxation age forming of AA6082 with elastic and plastic loadings. J Mater. Process. Tech. 2021;295:117168. https://doi.org/10.1016/j.jmatprotec.2021.117168.

[5] Su HL, Huang L, Li JJ, Xiao W, Zhu H, Feng F, Li HW, Yan SL. Formability of AA 2219-O sheet under quasi-static, electromagnetic dynamic, and mechanical dynamic tensile loadings. J. Mater. Sci. Tech. 2021;70:125–35. https://doi.org/10.1016/j.jmst.2020.07.023.

[6] Biesuz M, Saunders T, Ke D, Reece MJ, Hu CF, Grasso S. A review of electromagnetic processing of materials (EPM): heating, sintering, joining and forming. J. Mater Sci. Tech. 2021;69:239–72. https://doi.org/10.1016/j.jmst.2020.06.049.

[7] Xie BX, Huang L, Xu JH, Wang Y, Xu YK, Zhang HP, Li JJ. Deformation behavior and formability of solid solution state Al–Li alloy in electromagnetic forming. Mater. Sci. Eng. A. 2022;854:143858. https://doi.org/10.1016/j.msea.2022.143858.

[8] Li MQ, Shen YD, Luo K, An Q, Gao P, Xiao PH, Zou Y. Harnessing dislocation motion using an electric field. Nat Mater 2023;22:958–63. https://doi.org/10.1038/s41563-023-01572-7.

[9] Li CZ, Xu ZT, Peng LF, Lai XM. An electric-pulse-assisted stamping process towards springback suppression and precision fabrication of micro channels. Int J Mech Sci 2022;218:107081. https://doi.org/10.1016/j.ijmecsci.2022.107081.

[10] Shi CC, Zhang KF, Lu Z, Xiao H. Microstructure evolution and mechanical properties of Ti46. 5Al2Cr1. 8Nb-(W, B) alloys fabricated by spark plasma sintering and pulse current assisted isothermal forging. Mater. Sci. Eng. A. 2019;747:98–110. https://doi.org/10.1016/j.msea.2019.01.062.

[11] Xiao H, Lu Z, Zhang KF, Jiang SS, Shi CC. Achieving outstanding combination of strength and ductility of the Al-Mg-Li alloy by cold rolling combined with electropulsing assisted treatment. Mater Des 2020;186:108279. https://doi.org/10.1016/j.matdes.2019.108279.

[12] Troitskii OA. The effect of additional plastification of irradiated metal with current pickup. Strength Mater 1975;7(1):36–9. https://doi.org/10.1007/BF01522457.

[13] Troitskii OA, Spitsyn VI, Sokolov NV, Ryzhkov VG. Electroplasticity drawing of stainless steels. Dokl Akad Nauk SSSR 1977;237(5):1082–5.

[14] Troitskii OA, Spitsyn VI, Sokolov NV, Ryzhkov VG. Application of high-density current in plastic working of metals. Phys. Status Solidi A 1979;52(1):85–93. https://doi.org/10.1002/pssa.2210520109.

[15] Sprecher AF, Mannan SL, Conrad H. Overview no. 49: on the mechanisms for the electroplastic effect in metals. Acta Metall 1986;34(7):1145–62. https://doi.org/10.1016/0001-6160(86)90001-5.

[16] Ross CD, Irvin DB, Roth JT. Manufacturing aspects relating to the effects of direct current on the tensile properties of metals. ASME J. Eng. Mater. Tech. 2007;129(2):342–7. https://doi.org/10.1115/1.2712470.

[17] Perkins TA, Kronenberger TJ, Roth JT. Metallic forging using electrical flow as an alternative to warm/hot working. ASME J. Manuf. Sci. Eng. 2007;129(1):84–94. https://doi.org/10.1115/1.2386164.

[18] Roth JT, Loker I, Mauck D. Enhanced formability of 5754 aluminum sheet metal using electric pulsing. Trans. of the North American Manuf. Res. Institution. of SME. 2008;36:405–12.

[19] Salandro WA, Jones JJ, McNeal TA, Roth JT, Hong ST, Smith MT. Formability of Al 5xxx sheet metals using pulsed current for various heat treatments. ASME J. Manuf. Sci. Eng. 2010;132(5):1–11. https://doi.org/10.1115/1.4002185.

[20] Zhou C, Zhan LH, Li H, Liu CH, Xu YQ, Ma BL, Yang YL, Huang MH. Dislocation reconfiguration during creep deformation of an Al-Cu-Li alloy via electropulsing. J. Mater. Sci. Tech. 2022;130:27–34. https://doi.org/10.1016/j.jmst.2022.05.008.

[21] Lee T, Magargee J, Ng MK, Cao J. Constitutive analysis of electrically-assisted tensile deformation of CP-Ti based on non-uniform thermal expansion, plastic softening and dynamic strain aging. Int J Plast 2017;94:44–56. https://doi.org/10.1016/j.ijplas.2017.02.012.

[22] Kim MJ, Jeong HJ, Park JW, Hong ST, Han HN. Modified Johnson-Cook model incorporated with electroplasticity for uniaxial tension under a pulsed electric current. Metal. Mater. Inter. 2018;24:42–50. https://doi.org/10.1007/s12540-017-7297-1.

[23] Kim MJ, Yoon S, Park S, Jeong HJ, Park JW, Kim K, Jo J, Heo T, Hong ST, Cho SH, Kwon YK, Choi IS, Kim M, Han HN. Elucidating the origin of electroplasticity in metallic materials. Appl Mater Today 2020;21:100874. https://doi.org/10.1016/j.apmt.2020.100874.

[24] Liu XB, Zhang D, Wang H, Yan Y, Zhang XF. Regulating solute partitioning utilized to decorate grain boundary for improving corrosion resistance in a model Al-Cu-Mg alloy. Corros. Sci. 2021;181:109219. https://doi.org/10.1016/j.corsci.2020.109219.

[25] Qin SY, Zhang XF. Ultrafast regulation of nano-scale matrix defects using electrical property discrepancies to delay material embrittlement. J. Mater. Sci. Tech. 2022;119:25–36. https://doi.org/10.1016/j.jmst.2021.11.070.

[26] Zhao S, Zhang R, Chong Y, Li XQ, Odeh AA, Rothchild E, Chrzan DC, Asta M, Jr JWM, Minor AM. Defect reconfiguration in a Ti–Al alloy via electroplasticity. Nat Mater 2021;20(4):468–72. https://doi.org/10.1038/s41563-020-00817-z.

[27] Wu WL, Song YL, Lu J, Yu YQ, Hua L. Novel strategy of electroshock treatment for improving mechanical performances of Al–Zn–Mg–Cu alloy by edge dislocation increment. Mater. Sci. Eng. A. 2022;854:143805. https://doi.org/10.1016/j.msea.2022.143805.

[28] Okazaki K, Kagawa M, Conrad H. Effects of strain rate, temperature and interstitial content on the electroplastic effect in titanium. Scr. Metall. 1979;13(6):473–7. https://doi.org/10.1016/0036-9748(79)90072-3.

[29] Pan L, He W, Gu BP. Effects of electric current pulses on mechanical properties and microstructures of as-quenched medium carbon steel. Mater. Sci. Eng. A. 2016;662:404–11. https://doi.org/10.1016/j.msea.2016.03.031.

[30] Yi K, Zhou S, Zhang XF. Suppression of serrated flow in medium Mn steel under pulsed electric current. Mater. Sci. Eng. A. 2022;846:143271. https://doi.org/10.1016/j.msea.2022.143271.

[31] Li XQ, Turner J, Bustillo K, Minor AM. In situ transmission electron microscopy investigation of electroplasticity in single crystal nickel. Acta Mater 2022;223:117461. https://doi.org/10.1016/j.actamat.2021.117461.

[32] Molotskii MI. Theoretical basis for electro-and magnetoplasticity. Mater. Sci. Eng. A. 2000;287(2):248–58. https://doi.org/10.1016/S0921-5093(00)00782-6.

[33] Tiwari J, Pratheesh P, Bembalge OB, Krishnaswamy H, Amirthalingam M, Panigrahi SK. Microstructure dependent electroplastic effect in AA 6063 alloy and its nanocomposites. J Mater Res Technol 2021;12:2185–204. https://doi.org/10.1016/j.jmrt.2021.03.112.

[34] Li X, Zhu Q, Hong YR, Zheng H, Wang J, Wang JW, Zhang Z. Revealing the pulse-induced electroplasticity by decoupling electron wind force. Nat Commun 2022;13(1):6503. https://doi.org/10.1038/s41467-022-34333-2.

[35] Krasnikov VS, Mayer AE, Pogorelko VV. Prediction of the shear strength of aluminum with θ phase inclusions based on precipitate statistics, dislocation and molecular dynamics. Int J Plast 2020;128:102672. https://doi.org/10.1016/j.ijplas.2020.102672.

[36] Santos-Güemes R, Bellón B, Esteban-Manzanares G, Segurado J, Capolungo L, Llorca J. Multiscale modelling of precipitation hardening in Al–Cu alloys: dislocation dynamics simulations and experimental validation. Acta Mater 2020;188:475–85. https://doi.org/10.1016/j.actamat.2020.02.019.

[37] Roh JH, Seo JJ, Hong ST, Kim MJ, Han HN, Roth JT. The mechanical behavior of 5052-H32 aluminum alloys under a pulsed electric current. Int J Plast 2014;58:84–99. https://doi.org/10.1016/j.ijplas.2014.02.002.

[38] Wang XW, Xu J, Shan DB, Guo B, Cao J. Modeling of thermal and mechanical behavior of a magnesium alloy AZ31 during electrically-assisted micro-tension. Int J Plast 2016;85:230–57. https://doi.org/10.1016/j.ijplas.2016.07.008.

[39] Kim MJ, Lee MG, Hariharan K, Hong ST, Choi IS, Kim DY, Oh KH, Han HN. Electric current–assisted deformation behavior of Al-Mg-Si alloy under uniaxial tension. Int J Plast 2017;94:148–70. https://doi.org/10.1016/j.ijplas.2016.09.010.
[40] Liu YZ, Wan M, Meng B. Multiscale modeling of coupling mechanisms in electrically assisted deformation of ultrathin sheets: an example on a nickel-based superalloy. Int. J. Mach. Tool. Manu. 2021;162:103689. https://doi.org/10.1016/j.ijmachtools.2021.103689.
[41] Zhao YC, Wan M, Meng B, Xu J, Shan DB. Pulsed current assisted forming of ultrathin superalloy sheet: experimentation and modelling. Mater. Sci. Eng. A. 2019;767:138412. https://doi.org/10.1016/j.msea.2019.138412.
[42] Gao J, Li HW, Sun XX, Zhang X, Zhan M. Electro-thermal-mechanical coupled crystal plasticity modeling of Ni-based superalloy during electrically assisted deformation. Int J Plast 2022;157:103397. https://doi.org/10.1016/j.ijplas.2022.103397.
[43] Rauch EF, Gracio JJ, Barlat F. Work-hardening model for polycrystalline metals under strain reversal at large strains. Acta Mater 2007;55(9):2939–48. https://doi.org/10.1016/j.actamat.2007.01.003.
[44] Hariharan K, Kim MJ, Hong ST, Kim D, Song JH, Lee MG, Han HN. Electroplastic behaviour in an aluminium alloy and dislocation density based modelling. Mater Des 2017;124:131–42. https://doi.org/10.1016/j.matdes.2017.03.072.
[45] Tiwari J, Balaji V, Krishnaswamy H, Amirthalingam M. Dislocation density based modelling of electrically assisted deformation process by finite element approach. Int J Mech Sci 2022;227:107433. https://doi.org/10.1016/j.ijmecsci.2022.107433.
[46] Song YL, Wang ZQ, Yu YQ, Wu WL, Wang ZM, Lu J, Sun Q, Xie LC, Hua L. Fatigue life improvement of TC11 titanium alloy by novel electroshock treatment. Mater Des 2022;221:110902. https://doi.org/10.1016/j.matdes.2022.110902.
[47] Wu WL, Song YL, Zhou P, Yu YQ, Xie LC, Hua L. Mechanical properties improvement of pre-deformed Al–Zn–Mg–Cu alloys by electroshocking treatment based on the non-equilibrium scattering of electron-dislocation. J. Alloy. Compd. 2021;861:157987. https://doi.org/10.1016/j.jallcom.2020.157987.
[48] Yang Y, Qin RS, Dong YL, Wang J, Ye C. Crystal plasticity modeling of electropulsing induced plasticity in metals. Inter. J. Plast. 2023;103828. https://doi.org/10.1016/j.ijplas.2023.103828.
[49] Xu ZT, Li XN, Zhang R, Ma J, Qiu DK, Peng LF. The effect of electric current on dislocation activity in pure aluminum: a 3D discrete dislocation dynamics study. Int J Plast 2023:103826. https://doi.org/10.1016/j.ijplas.2023.103826.
[50] Kreyca J, Kozeschnik E. State parameter-based constitutive modelling of stress strain curves in Al-Mg solid solutions. Int J Plast 2018;103:67–80. https://doi.org/10.1016/j.ijplas.2018.01.001.
[51] Wang XW, Wang CJ, Liu Y, Liu C, Wang ZL, Guo B, Shan DB. An energy based modeling for the acoustic softening effect on the Hall-Petch behavior of pure titanium in ultrasonic vibration assisted micro-tension. Int J Plast 2021;136:102879. https://doi.org/10.1016/j.ijplas.2020.102879.
[52] Hunter A, Preston DL. Analytic model of dislocation density evolution in fcc polycrystals accounting for dislocation generation, storage, and dynamic recovery mechanisms. Int J Plast 2022;151:103178. https://doi.org/10.1016/j.ijplas.2021.103178.
[53] Taylor GI. Plastic strain in metals. J Inst Met 1938;62:307–24.
[54] Poorganji B, Sepehrband P, Jin H, Esmaeili S. Effect of cold work and non-isothermal annealing on the recrystallization behavior and texture evolution of a precipitation-hardenable aluminum alloy. Scr. Mater. 2010;63(12):1157–60. https://doi.org/10.1016/j.scriptamat.2010.08.014.
[55] Kuo CM, Lin CH, Huang YC. Plastic deformation mechanism of pure copper at low homologous temperatures. Mater. Sci. Eng. A. 2005;396(1):360–8. https://doi.org/10.1016/j.msea.2005.01.052.
[56] Kocks UF. Constitutive behavior based on crystal plasticity. London: Elsevier Applied Science; 1987. p. 1–88.
[57] Yao ZH, Kim GY, Wang ZH, Faidley LA, Zou QZ, Mei DQ, Chen ZC. Acoustic softening and residual hardening in aluminum: modeling and experiments. Int J Plast 2012;39:75–87. https://doi.org/10.1016/j.ijplas.2012.06.003.
[58] Krausz AS, Krausz K. Unified constitutive laws of plastic deformation. San Diego: Academic Press; 1996.
[59] Estrin Y. Dislocation-density-related constitutive modeling. Unified constitutive laws of plastic deformation 1996;1:69–106.
[60] Xiang S, Zhang X. Dislocation structure evolution under electroplastic effect. Mater. Sci. Eng. A. 2019;761:138026. https://doi.org/10.1016/j.msea.2019.138026.
[61] Tiwari J, Balaji V, Krishnaswamy H, Amirthalingam M. Dislocation density based modelling of electrically assisted deformation process by finite element approach. Int J Mech Sci 2022;227:107433. https://doi.org/10.1016/j.ijmecsci.2022.107433.
[62] Fan R, Magargee J, Hu P, Jian C. Influence of grain size and grain boundaries on the thermal and mechanical behavior of 70/30 brass under electrically-assisted deformation. Mater. Sci. Eng. A. 2013;574:218–25. https://doi.org/10.1016/j.msea.2013.02.066.
[63] Conrad H. Electroplasticity in metals and ceramics. Mater. Sci. Eng. A. 2000;287(2):276–87. https://doi.org/10.1016/S0921-5093(00)00786-3.
[64] Kim MJ, Lee K, Oh KH, Choi Is, Yu HH, Hong ST, Han HN. Electric current-induced annealing during uniaxial tension of aluminum alloy. Scr. Mater. 2014;75:58–61. https://doi.org/10.1016/j.scriptamat.2013.11.019.
[65] Ding HP, Gong P, Chen W, Peng Z, Bu HT, Zhang M, Tang XF, Jin JS, Deng L, Xie GQ, Wang XY, Yao KF, Schroers J. Achieving strength-ductility synergy in metallic glasses via electric current-enhanced structural fluctuations. Int J Plast 2023;103711. https://doi.org/10.1016/j.ijplas.2023.103711.
[66] Kir'yanchev NE, Troitskii OA, Klevtsur SA. Electroplastic deformation of metals. Strength Mater 1983;15(5):709–15. https://doi.org/10.1007/BF01523224 (review).
[67] Frost HJ, Ashby MF. Deformation-mechanism maps: the plasticity and creep of metals and ceramics. first ed. Oxford: Pergamon Press; 1982.
[68] Fran OISD, Pineau A, Zaoui A. Mechanical behavior of materials. Dordrecht: Kluwer Academic Publishers; 1998.